To the Graduate Council:

I am submitting herewith a thesis written by Michael Alberto Guillorn entitled "Fabrication of Dissimilar Metal Electrodes with Nanometer Interelectrode Distance Suitable for the Electrical Characterization of Molecular-Scale Electronic Devices." I have examined the final copy of this thesis for form and content and recommend that it be accepted in partial fulfillment of the requirements for the degree of Master of Science, with a major in Electrical Engineering.

James Rochelle

James Rochelle, Major Professor

We have read this thesis
and recommend its acceptance:

Michael L Simpson

Syed Kamrul Islam

Accepted for the Council:

Interim Vice Provost and
Dean of the Graduate School

Fabrication of Dissimilar Metal Electrodes with Nanometer Interelectrode Distance Suitable for the Electrical Characterization of Molecular-Scale Electronic Devices

A Thesis

Presented for the

Master of Science Degree

The University of Tennessee, Knoxville

Michael A. Guillorn

August 2000

Acknowledgements

This thesis would not have been possible without the help of several people who have been in my life for sometime or been featured prominently in it over the past few years. Foremost, I would like to thank my advisor Dr. Michael Simpson for providing me with excellent advice and an interesting research project that has lead to many wonderful advances both scientific and personal. Secondly, I need to thank Dr. Elıas Greenbaum, Dr. Ida Lee and Dr. James Lee for performing the groundbreaking work in the area of molecular-scale electronics that served as the catalyst for this research project. I would also like to thank Dr. James Rochelle, Dr. Syed Islam, Dr. Douglas Lowndes, Dr. Gyula Eres, Dr. David Joy and the staff of the Monolithic Systems Development group of the Instrumentation and Controls division at the Oak Ridge National Laboratory Their helpful discussions and assistance on various matters throughout the course of this work was greatly appreciated.

Much of this work was performed at the Cornell Nanofabrication Facility (CNF) at Cornell University in Ithaca, New York. This is a truly magical place where miracles of modern science occur on a daily basis. I wish to thank the entire staff of this facility for their support. However, I owe a debt of gratitude to Dr. Richard Tiberio and Dr. Dustin Carr for their help in developing the fabrication processes used in this research and teaching me the art and science of direct write electron beam lithography and nanofabrication.

I am also indebted to Megan Shea for providing me with an ample supply of love and motivation and to my sister, Lysbeth Guillorn, for having a profound positive influence on my life. Finally I wish to thank the creator for giving us this wonderful world, the inquisitive nature that drives us to explore every facet of it and most of all for giving us music. Without listening to and playing music in its various styles and forms I would not have been able to finish high school, let alone this thesis.

This work was funded by the Laboratory Director's Research and Development Funding Program of the Oak Ridge National Laboratory and the Defense Advanced Research Projects Agency under contract number DE-AC05-96OR22464.

Abstract

As complementary metal-oxide-semiconductor (CMOS) based integrated circuits (IC's) approach the physical and economic limit of performance enhancement through device scaling the need for a new paradigm to realize nanoscale electronic devices is ever increasing. One proposed architecture for realizing the next generation of IC's involves the use of molecular monolayers and single molecules as active electronic components commonly referred to as molecular-scale electronics. Several such devices have been demonstrated using a host of novel electrical characterization structures and techniques.

In this thesis a controllable and reproducible process for fabricating electrode pairs suitable for probing the electrical properties of potential molecular-scale electronic devices is presented. This process is capable of fabricating dissimilar metal electrodes with a minimum interelectrode distance of less than 6 nm using electron beam lithography and liftoff pattern transfer. Electrode structures employing pairs of Au or AuPd electrodes and a dissimilar metal electrode were fabricated in three different patterns. 300 μm long parallel electrode structures with interelectrode distances as low as 10 nm, 75 nm wide electrode pairs with interelectrode distances lower than 6 nm, and a multi-terminal electrode structure with reproducible interelectrode distances of 8 nm were realized using this technique. The processing issues associated with the fabrication of these structures are discussed along with the intended application of these devices.

Table of Contents

Chapter Page

List of Figure

Figure Page

Abbreviations

ACE	Acetone
AFM	Atomic Force Microscopy
CAD	Computer Aided Design
CMOS	Complementary Metal Oxide Semiconductor
DAC	Digital to Analog Converter
DiMEND	Dissimilar Metal Electrodes with Nanometer Interelectrode Distance
DUV	Deep Ultra Violet
EBL	Electron Beam Lithography
ESD	Electrostatic Discharge
ETV	Electron Transport Vector
FE	Field Emission
FM	focus mark
IC	Integrated Circuit
IPA	Isopropanol
ISEM	Integrated Scanning Electron Microscope
LB	Langmuir-Blodgett
MCB	Mechanically Controllable Breakjunction
MIBK	Methyl Isobutyl Ketone
MW	Molecular Weight
PG	Pattern Generator
PMMA	Polymethyl Methacrylate
PSI	Photosystem I
PVD	Physical Vapor Deposition
RIE	Reactive Ion Etching
SAM	Self-Assembled Monolayer
SEM	Scanning Electron Microscopy
SMU	Source Measurement Unit
STM	Scanning Tunneling Microscope
STS	Scanning Tunneling Spectroscopy
TFE	Thermal Field Emission
VB6	Leica Vector Beam 6 Electron Beam Lithography System
VLSI	Very Large Scale Integration

Chapter 1

Introduction

1.1 The Limits of CMOS and the Drive Towards Molecular Scale Electronics

The invention and development of CMOS transistor-based IC technology have had a tremendous and enduring impact worldwide over the past 25 years Consistent innovations in the science of CMOS IC fabrication have allowed the dimensions of these devices to be scaled down dramatically, increasing the transistor density per die area and device operating speed Moreover, aggressive device scaling has decreased the amount of power required by each transistor and reduced the total cost per device on an IC This ability to fabricate inexpensive CMOS-based very-large-scale integrated (VLSI) circuits catalyzed the computer revolution and brought the electronics industry to the forefront of the global economy. CMOS VLSI microprocessors lie at the heart of desktop computers, "smart" toasters and modern automobiles alike and have provided the basis for numerous scientific and technological breakthroughs in a plethora of fields of study[1]

The 1999 National Technology Roadmap for Semiconductors calls for an additional factor of 10^3 increase in computational efficiency[2] by the year 2008[3]. As stated above, the capability to decrease the minimum dimensions of CMOS transistors has been the primary force behind the rapid advances of VLSI-based technology Unfortunately, physical and economic phenomena are conspiring to make this particular

path toward fabricating less expensive and more powerful IC's a finite one It is projected that the evolution of CMOS technology will have run its course shortly after the year 2010 for a variety of reasons[4,5] The stated computational efficiency goal would then fall just beyond the reach of CMOS based IC technology—disregarding levels of performance that exist beyond this mark. It has recently been postulated that there are potentially eight orders of magnitude in computational energy efficiency beyond the limit of CMOS IC technology[6] These issues clearly indicate that a new paradigm for realizing the next generation of integrated circuits must be found

In Richard Feynman's historic speech "There's Plenty of Room at the Bottom" given at the December meeting of the American Physical Society in 1959, the concept of nanotechnology was first presented to the scientific world[7] In his talk, Feynman brought forth the idea that the ultimate level of device integration for computing purposes would involve individual components no bigger than 10 nm wide forming entire circuits realized in areas a few thousand angstroms across These ideas have provided the inspiration for many researchers from a variety of disciplines to embark on a quest to realize nanoscale electronic devices One proposed method of achieving device integration on this level involves the use of molecular monolayers and single molecules as active electronic components This approach is more commonly referred to as molecular electronics

1.1.1 Molecular Electronic Devices

The first serious proposal for realizing a molecular electronic device, a molecular rectifier, was made by Aviram and Ratner in 1974[8] In this visionary work they theorized that a bilayer of electron donor and acceptor molecules separated by a potential barrier trapped between two metal electrodes would function in an analogous manner to a PN-junction rectifier The general idea of their work was based on the principle that charge transport through a molecular layer will occur via tunneling. They hypothesized that the molecular energy levels (molecular orbitals) of a π-conjugated molecule would participate in the tunneling process and be energetically close to the Fermi level of the electrode metals[9]. Placing a sufficient level of external bias voltage on the electrodes, the Fermi level of the metals could be brought into resonance with the molecular energy levels Due to the asymmetrical electrical characteristics of the molecular bilayer, resonance would be achieved with greater facility for one bias polarity than for the other creating a rectifying junction

Following the theoretical work of Aviram and Ratner several molecular rectifiers based on π-conjugated systems[10,11,12], other forms of molecular bridges[13,14], and biomolecules[15] have been demonstrated All of these devices show current rectification properties similar to PN junction diodes and yet are smaller than traditionally fabricated PN junctions by an average factor of 10^6. Other demonstrated molecular electronic components include molecular wires[16], a resonant tunneling diode[17] and a negative differential resistance device[18] It should be noted that there is another category of

molecular electronic devices composed of graphite-like carbon-based materials such as C_{60} Fullerenes and the ubiquitous carbon nanotube (CNT) A discussion of these devices and the issues associated with electrically characterizing them is beyond the scope of this thesis Several excellent introductory texts and review papers[19] exploring this topic are available.

1.2 Electrically Characterizing Molecular Junctions

With the marked decrease in dimensions of molecular electronic devices also comes a sharp increase in the level of difficulty associated with performing their electrical characterization. As with any electronic device, the behavior of a molecular electronic device must be fully understood before it is used in an electrical circuit. Its response to DC as well as AC excitations needs to be determined, understood, modeled and incorporated into analytical tools that will facilitate the design of circuits as well as allow for their simulation.

Most molecules that possess electrical properties of interest have critical dimensions somewhere between 1 nm and 10 nm[9,15]. It follows that if one is going to study the properties of these molecules electrical probes capable of contacting objects this size are required Fabricating pairs of electrodes that have interelectrode distances within this size regime is not a trivial task as it exceeds the resolution limit of traditional photolithography and deep ultra violet (DUV) lithography and surpasses the performance limit of X-ray lithography tools. In principle, the resolution of X-ray lithography is quite

high, nominally 10Å, yet instrumentation issues serve to degrade the performance of these tools significantly. Until recently[37,38], the highest resolution lithography tool available, direct-write electron beam lithography (EBL) has also been incapable of repeatable production of electrodes with interelectrode distances on the order of 10 nm or less

It should be noted, EBL tools are constantly evolving Unlike photolithography, EBL is not fundamentally limited by the wavelength of light used in the exposure and instrumentation is readily available that makes EBL systems more robust than X-ray lithography machines. As the science and technology of electron field emission is improved, so is the quality of EBL systems.

Another issue associated with the measurement of the electrical properties of single molecules is deposition of the molecule under test into the test structure Provided that one can fabricate electrodes suitable for measuring a single molecular monolayer, it is another equally difficult task to place, position and then bind a molecule between the two contacts Mechanical probes able to manipulate single molecules simply do not exist Techniques such as "optical tweezers"[20] can manipulate objects with atomic dimensions, however they cannot fix them in place or control their orientation. What is required is a method of self-assembling these molecules into the measurement structure to create a metal/molecular monolayer/metal heterojunction.

1.2.1 Early Measurement Techniques

The first techniques developed for performing electrical measurements on single or small groups of molecules typically fit into one of two categories, both of which bypassed the resolution limits of lithography-based fabrication entirely. The first method is useful only when characterizing molecules that can be arrayed in a Langmuir-Blodgett (LB) thin film LB thin films are dense and highly ordered monolayers of molecules often likened to a liquid crystal lattice[21] These properties allow LB films to be deposited into vertical metal/molecular monolayer/metal "sandwich" structures formed as follows A LB thin film is first deposited onto a metal electrode previously patterned on a nonconducting substrate. Provided that the electrode area is sufficiently small, the LB film will uniformly cover the electrode without leaving any vacancies in the molecular monolayer A second metal electrode can then be deposited on top of the LB film creating a vertical two-terminal test structure[11] (refer to figure 1-1) Unfortunately, this technique is of little use for performing measurements on molecular monolayers that cannot be arrayed in LB thin films[22] Any monolayer that may possess vacancies runs a high risk of being shorted out by the upper and lower electrode during the second electrode's deposition preventing any sort of useful measurement from occurring.

The second method, which has been used to conduct a great number of electrical measurements on single molecules, employs the use of a scanning tunneling microscope (STM) in a technique known as scanning tunneling spectroscopy (STS) In these types of measurements a molecular monolayer or a suspension of single molecules can be

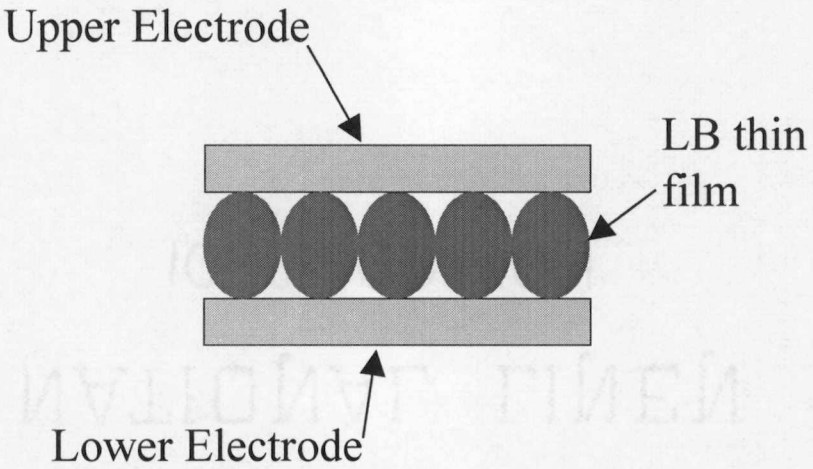

Figure 1-1: Diagram of LB thin film "sandwich" measurement technique.

adsorbed onto a conductive substrate. The STM tip can then be brought directly over an individual molecule and used to make conductance measurements by sweeping the bias voltage of the substrate with respect to the tip and measuring the resultant tunneling current (refer to figure 1-2) General examples of this technique can be found in the literature[13-15]. This technique is limited by the inherent tunneling gap between the STM tip and the molecule and offers no means for making measurements on multiple molecules arranged in series or parallel.

1.2.2 Techniques for Fabricating Metal/Self-Assembled Monolayer/Metal Heterojunctions

The deficiencies of traditional photolithography-based fabrication techniques and the limited scope of the previously discussed measurement methods have forced researchers in the molecular electronics field to pioneer new techniques in nanofabrication technology. Over the past five years there has been a rapid increase of activity in the field of electrically characterizing molecular junctions At the forefront of this boom has been Mark Reed's group at Yale University Stemming from their study of charge transport through metallic point contacts, a technique which exploits the atomically sharp nature of mechanically induced breaks in metal wire was developed, known as the mechanically controllable break junction (MCB)[23]. This technique was used to perform one of the first non-STM based electrical measurement on a single molecule reported in 1997[24]

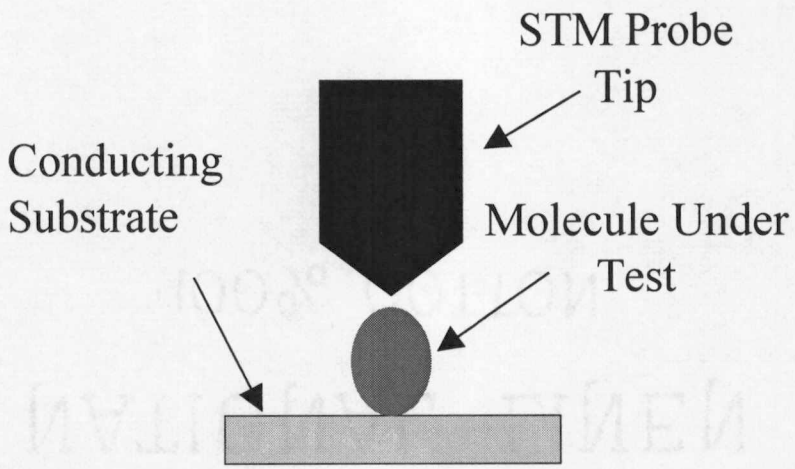

Figure 1-2: Diagram of STM based measurement technique

The operating principle of the MCB is quite simple A 200μm diameter Au wire is notched almost to the point of shear using a razor blade. Epoxy is then used to cement the wire on both sides of the notch to a thin phosphor-bronze bending bar coated with an insulating foil Centering the structure between two counter supports, a piezoelectric micromanipulator is then used to apply force to the backside of the bending bar (refer to figure 1-3). By adjusting the micromanipulator's coarse position the wire will break forming two atomically sharp Au electrodes Then, by monitoring the conductance of the wire it is possible to adjust the distance between the electrodes with angstrom resolution utilizing the piezoelectric element This precise control in the interelectrode distance is made possible via a mechanical reduction factor in the displacement of the piezoelectric element caused by the bending bar.

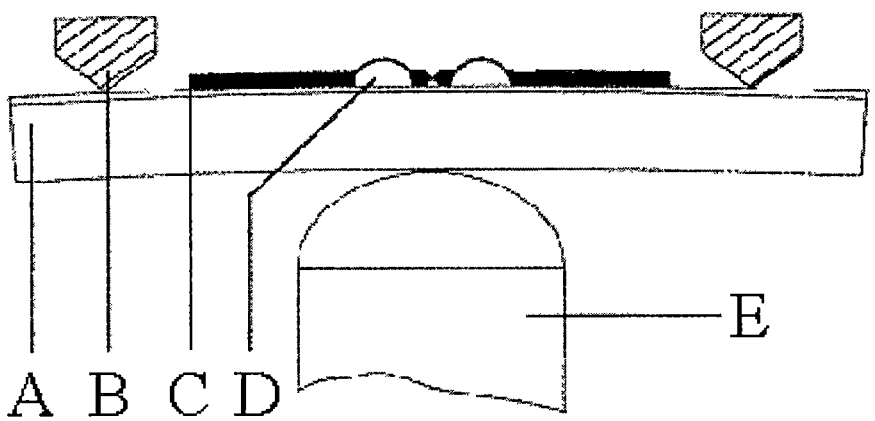

Figure 1-3. A schematic of the MCB junction with (A) the bending beam, (B) the counter supports, (C) the notched gold wire, (D) the glue contacts, (E) the piezo[24]

Chemical modification of Au substrates via alkane-thiol chains have been shown to aid in the self-assembly of molecules to metal surfaces[25] By using Au as the electrode material of the MCB these self-assembly techniques were successfully employed by Reed's group to deposit organic-synthetic molecules onto the electrodes Using the piezoelectric element the interelectrode distance was adjusted until the electrodes formed a direct metal/molecule/metal heterojunction (refer to figure 1-4).

The MCB technique is inherently stable, easy to operate and produce, and is adjustable However, it also requires a large external apparatus, and can only be used to fabricate pairs of electrodes of a single metal. The latter of these two deficiencies is indicative of a problem endemic to many of the measurement techniques demonstrated in the literature It is possible to deposit symmetric organic-synthetic molecules in between properly spaced Au electrodes using alkane-thiol self-assembly techniques and then electrically characterize them because the orientation of the molecules between the electrodes does not effect the measurement. Asymmetric molecules, however, cannot be examined using such devices An example of this type of molecule is the photosystem I (PSI) reaction center which is of demonstrated interest to molecular electronics research[15]

Self-assembly techniques have been developed to preferentially orient the PSI with respect to a Au substrate. The polar nature of this molecule inhibits the use of the MCB for the formation of Au/PSI/Au heterojunctions (refer to figure 1-5). A molecular monolayer will be formed on both of the Au electrodes, as the interelectrode distance is closed, molecules bridging the gap will be oriented in both directions preventing any

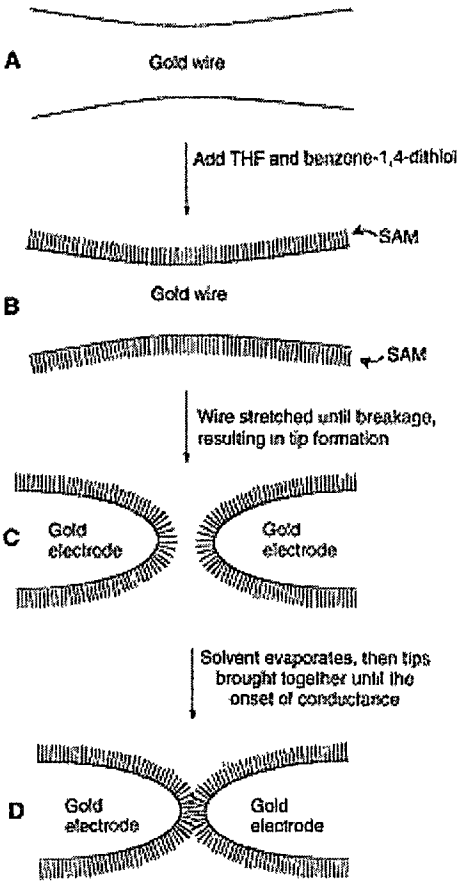

Figure 1-4 Schematic of the MCB based measurement process. (A) The gold wire of the break junction before breaking and tip formation (B) After addition of benzene-1,4-dithiol, SAMs form on the gold wire surfaces (C) Mechanical breakage of the wire in solution produces two opposing gold contacts that are SAM-covered (D) After the solvent is evaporated, the gold contacts are slowly moved together until the onset of conductance is achieved[24]

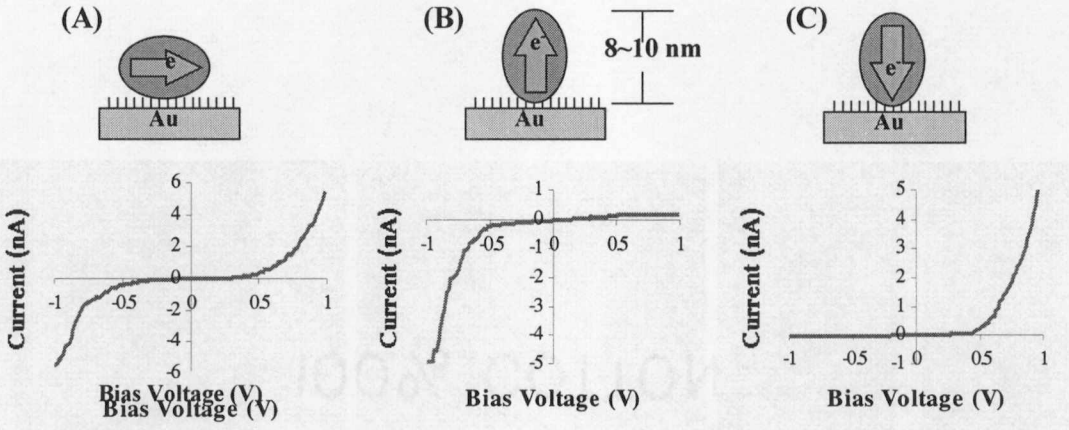

Figure 1-5: The PSI biomolecule is an example of an asymmetric molecule with electrical properties of demonstrated interest to the molecular electronics community. (A), (B) and (C) show the directional dependence of the I-V characteristics of the PSI molecule[15].

meaningful measurement from occurring Electrode pairs composed of dissimilar metal electrodes, where only one member of the pair reacts with the thiol SAM would be ideally suited to the task of electrically characterizing these asymmetric molecules. Preferential self-assembly of the molecular monolayers should be possible in such a structure

Break junctions formed by electrostatic discharge (ESD) were shown to produce inter-electrode distances on the order of 1 nm to 10 nm[26] Using EBL and liftoff pattern transfer Au electrodes were defined such that the ends overlapped by a distance of less than 10nm. By driving a sufficiently high current through the electrodes the tips break at the overlap leaving a nanometer sized space in between the two Au electrodes

This technique surmounts the instrumentation problem of the MCB in that it is fully integrated and requires no external apparatus once the break is induced It may also be extended to fabricating electrode pairs of dissimilar metals. However, the interelectrode distance cannot be controlled as precisely as the MCB and cannot be fabricated in a wide variety of sizes At this time this technique has only been used to realize nanocrystal based single electron transistors. However it has the potential to be used to study transport through molecular junctions

A technique developed in the late 1980's by a group at Cornell[27] formed the basis of another novel measurement structure employed by Reed's group, dubbed the "nanopore" [18,28]. This structure consists of a nanometer-sized hole punched through a Si_3N_4 membrane with Au contacts above and below the opening separated by a distance

of a few nanometers It realizes a vertical metal/molecular monolayer/metal heterostructure similar to the metal/LB thin film/metal structure discussed earlier (refer to figure 1-6) The key difference is that the molecular monolayer under test does not need to be a LB thin film The problems inherent in the metal/LB thin film/metal technique described earlier for non-LB SAM's were circumvented by two aspects of the nanopore fabrication process. First, the ability to fabricate a measurement structure smaller than the domain size of the SAM forces the adsorbed monolayer to be highly ordered and primarily defect free[29]. Also, several precautionary measures are incorporated into the second electrode deposition process to safeguard against contact shorting between electrodes.

The nanopore technique was used to make stable electrical contact to a 4-thioacetylbiphenyl SAM and produce repeatable electrical measurements for extended periods of time showing that it behaves analogously to a PN junction diode[28]. It was also used to measure a molecule containing a nitroamine redox center showing a current-voltage response which exhibited a negative differential resistance [18] This work offers a significant tool for measuring non-LB SAM's including those comprised of asymmetric molecules Regretably, these structures require a complex fabrication process that is time consuming and involves several novel techniques thus limiting its usefulness.

C Dekker, *et al*[30], demonstrated a novel method for fabricating electrodes with an interelectrode distance as small as 4 nm in 1997 An oxidized silicon substrate with a thin coating of low-stress Si_3N_4 is used as a starting material. Polymethyl methacrylate (PMMA)[31] is then spun onto the material and EBL is used to pattern a long narrow slit

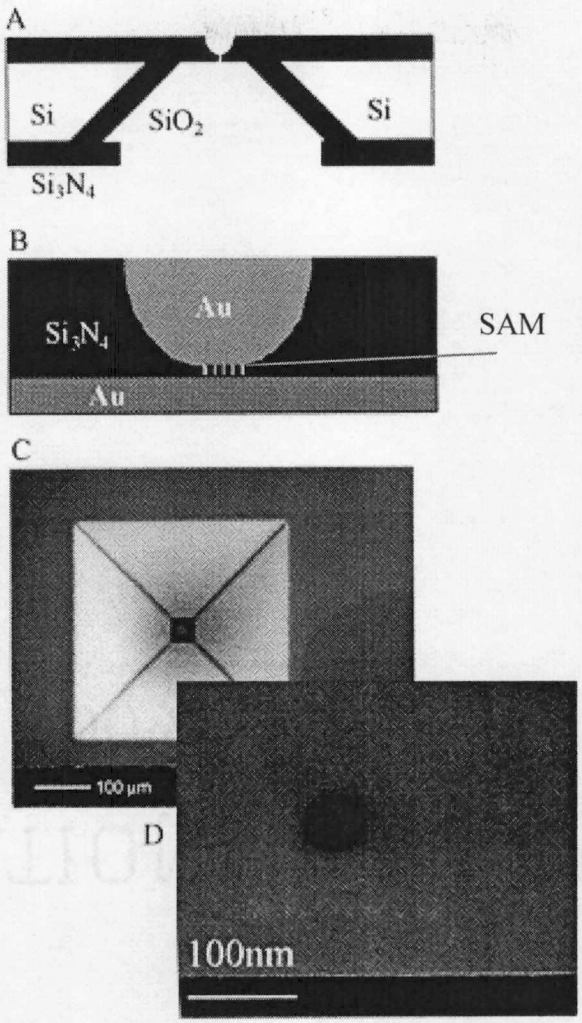

Figure 1-6: Electron micrographs showing nanopore fabrication. (A) Cross section of a silicon wafer with a nanopore etched through a suspended silicon nitride membrane. (B) Au-SAM-Au junction in the pore area. (C) Scanning electron micrograph (SEM) of pyramid Si structure after anisotropic Si etching [that is, the bottom view of (A)]. (D) SEM of an etched nanopore through the silicon nitride membrane[18].

roughly 100 nm wide with a local constriction of 20 nm. Reactive ion etching (RIE) of the Si_3N_4 layer followed by wet etching of the underlying SiO_2 produces two free-standing Si_3N_4 "fingers" at the constriction over a trench. These Si_3N_4 fingers are then coated with a fine-grained metal (such as Pt) to produce the actual metallic electrodes As the metal is deposited, the 20 nm constriction becomes narrower until it reaches the desired lower bound (refer to figure 1-7).

The homogeneous nature of the composition of the electrode pair inhibits the use of self-assembly techniques for the deposition of asymmetric molecules in this structure Dekker's group has developed a deposition technique involving the trapping of nanoscale materials in an electrostatic field generated between the two electrodes. An electrostatic field can be used to "catch" a highly polar nanoparticle This technique was verified by using it to self-assemble a Pd nanoparticle between the two electrodes However, it has yet to be successfully demonstrated on organic materials of interest to molecular electronics[32].

A technique known as offset mask (shadow mask or tilt mask) evaporation, first developed in the late 1970's[33] has been used to realize molecular electrical characterization structures This technique makes use of electron beam lithography (EBL) patterned resist as a physical evaporation mask. By evaporating metal at sufficiently oblique angles with respect to the substrate it is possible to realize multiple metal electrodes in a single patterned area due to the "shadow" created by the resist side-walls These electrodes have been realized with nanometer seperation and have been used primarily in the fabrication of single electron transistors[34] Repeatability has been

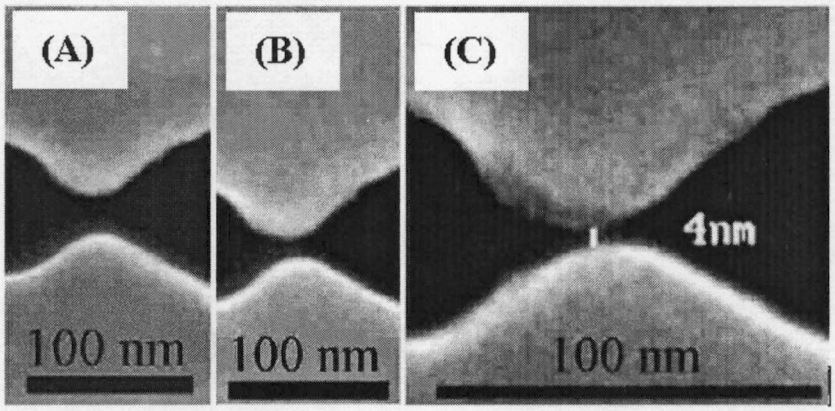

Figure 1-7: Electron micrographs of the Pt "fingers"; the gap between the electrodes can be slowly reduced to the desired small value by sputtering of additional layers of platinum. Here the gap was reduced from 25 nm (a) to 15 nm (b) and to 4 nm[30].

the limiting factor of this technique; the electrode geometry, interelectrode spacing and electrode placement are difficult to control[35]

In early 1999 a group at Stanford University demonstrated a fabrication technique involving the electrochemical plating of grossly spaced lithographically defined electrode pairs[36]. In this work EBL was used to define coarsely spaced electrodes of Au/Ti on an oxidized Si substrate. These structures were then placed in an aqueous solution consisting of 01 M potassium cyanaurate and a buffer composed of 1 M potassium bicarbonate and .2 M potassium hydroxide A Au pellet is then used as a counterelectrode connected in series with the patterned electrodes and a controllable voltage source. Coupling this circuit to a lock-in-amplifier connected in parallel with a resistor in series with the current source electrodeposition of the Au pellet can be driven by the controllable voltage source and monitored simultaneously. By measuring the interelectrode conductance the interelectrode distance can be ascertained and controlled. Inter-electrode distances as small as 1 nm were reported (refer to figure 1-8)

The ability to reproducibly fabricate planar electrode pairs with adjustable interelectrode distances down to 1 nm represents a breakthrough in molecular measurement. This technique surpasses the flexibility of the MCB and ESD break junctions and can be done at a fractional cost It is possible that electrodes of dissimilar metals can be fabricated by the electrochemistry of the deposition process producing an ideal test device for the electrical characterization of molecular junctions Furthermore, unlike the other techniques discussed thus far, it may be possible to fabricate multi-terminal test structures using this method, enabling the realization of functional molecular

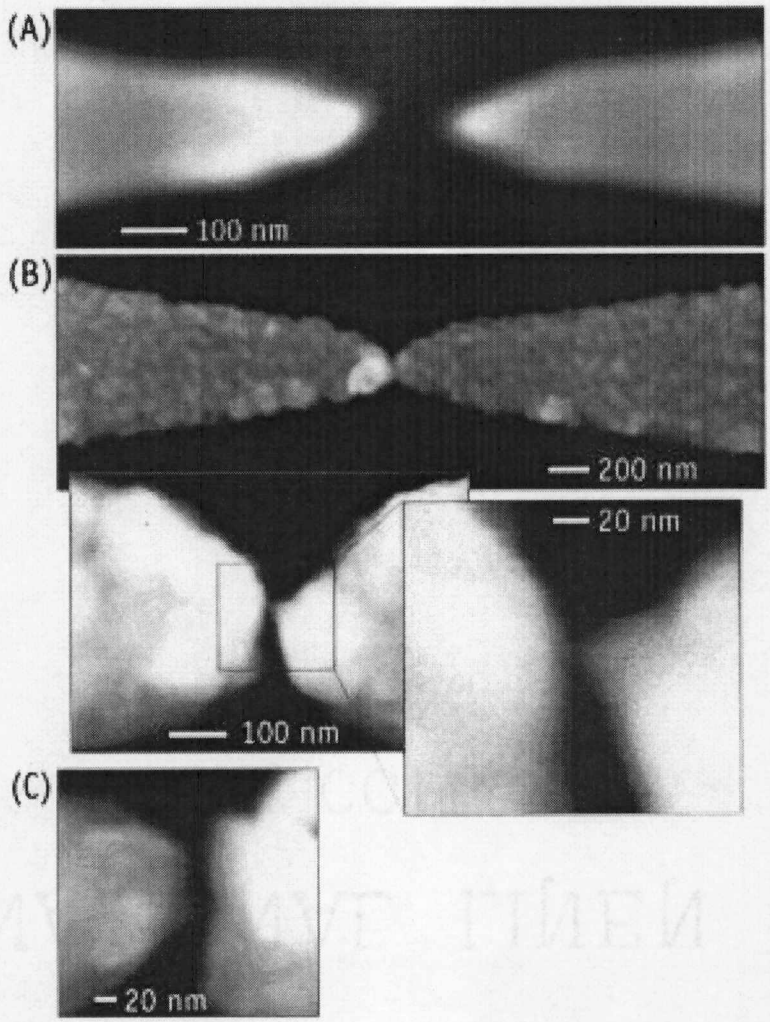

Figure 1-8: SEM images before and after electrodeposition (scale bars show dimensions). (A) Electrodes before electrodeposition. (B) Electrodes after electrodeposition.The resolution of the SEM is 5 nm, not sufficient to resolve the gap. (C) Electrodes in which the gap was reopened by electrodissolution[36].

scale logic devices One drawback of this technique is that the electrodeposited material will not adhere to the substrate in any manner, anchored only to the EBL defined electrode This may limit the overall robustness of the technique and put a potential distance limit on the length of the electrodeposited portion of the electrode pair[36].

1.3 The Use of High-Resolution EBL for the Fabrication of Molecular Electronic Device Electrical Characterization Structures

The ability to use EBL to fabricate electrodes suitable for the characterization of molecular monolayers would be an asset to this field of research, as it would bring with it the unparalleled level of flexibility and control commonly associated with EBL. The use of EBL to this end would permit electrode structures composed of a wide array of metals, in any number of patterns with an arbitrary number of measurement terminals, to be fabricated on a variety of substrates It was previously mentioned that direct-write EBL has been incapable of repeatable production of electrodes with interelectrode distances on the order of 10 nm or less Recent advances in EBL have begun to push these boundaries making the possibility of such a fabrication process feasible[37,38]

1.4 Thesis Objective

This thesis presents a flexible, controllable and reproducible process for fabricating dissimilar metal electrodes with nanometer interelectrode distance (DiMEND)

using high-resolution EBL and liftoff metallization processing This process is capable of realizing electrode pairs with a minimum interelectrode distance of 6 nm that allow thiol-based self-assembly techniques to be used to deposit asymmetric molecules into lateral metal/molecular monolayer/metal heterojunctions. This technique may also provide a method for demonstrating functional molecular logic gates on the nanoscale as it can be used to fabricate multi-terminal devices.

Chapter 2 will discuss the physics and technology of EBL and liftoff pattern transfer. Elements of electron optics, electron solid interactions and EBL systems will be presented. The chemistry of electron sensitive resists will be discussed along with its application to liftoff pattern transfer processes

In Chapter 3 the design of the DiMEND structures and their intended experimental use will be examined The properties of the Photosystem I molecule will be discussed to provide a context for the eventual application of the DiMENDs along with other design considerations that need to be addressed. The fabrication process developed for DiMEND production will be presented in Chapter 4 This chapter will provide a detailed summary of the processing steps followed to create the DiMEND structures in high yield. Chapter 5 will present the results of this fabrication process An assessment of the effectiveness of the DiMEND structures in terms of their ability to realize metal/molecular monolayer/metal heterojunction using self-assembly techniques will also be discussed. This work will be concluded in Chapter 6 with final comments on the presented topic.

Chapter 2

Electron Beam Lithography and Liftoff Pattern Transfer

2.1 Physics of Electron Beam Lithography

Electron beam lithography (EBL) systems are used in two general applications: mask writing and direct write lithography Fundamentally, both types of systems are the same, however some differences do exist in their electron beam generation and control mechanisms. The research work discussed in this Thesis was performed using a direct write EBL system; for the sake of being concise this chapter will be limited to a discussion of these types of systems. In order to understand how EBL systems function, it is necessary to acquire a rudimentary understanding of electron emission, electron optics, electron interactions with solids and the technology that has been developed to control these phenomena.

2.1.1 Electron Sources

The part of the EBL system that forms the electron beam is normally referred to as the column An EBL column typically consists of a series of several components starting with the electron source. All EBL systems require an electron source that has high intensity (high brightness), high uniformity, a small virtual source size, a limited spread of emitted electron energies, good stability and long life The most common

methods for extracting electrons from the source in an EBL system are heating a conducting filament (thermionic emission), applying a large electric field to a conducting needle point (cold field emission), or combining these two methods (thermally assisted field emission). In each of these types of sources the energy being added to the conducting material by the aforementioned means allows electrons to overcome the work function of the filament material and be emitted, typically into a vacuum of 10^{-6} Torr to 10^{-9} Torr.

Thermionic sources are standard for most low-end to moderately priced EBL systems due to its high brightness and relative stability. The beam current delivered by thermionic sources is dependent on the temperature of the cathode. Thermionic sources operating at high temperature can deliver greater beam current than field emission sources at the expense of an exponentially decreasing lifetime due to thermal evaporation of the cathode material LaB_6 cathodes operating at 1800 K are used frequently in thermionic EBL sources because of their exceptionally high current density and brightness.[39] However source lifetimes of 1000 hrs or less are common in systems employing LaB_6 filaments [40] This need to frequently replace the filament is a detriment in commercial production environments where more stable, longer life sources translate to less system downtime

Cold field emission (FE) sources have become common in electron microscopes due to their high brightness However, they have seen little use in commercial EBL systems due to their instability with regard to short-term noise as well as long term current drift. This is a serious problem in lithography processes where maintaining a

stable beam current plays an integral role in system performance and exposure uniformity. The noise seen in the emitted current from FE sources is caused by the adsorption of atoms onto the surface of the field emitter tip, affecting its work function and thus causing large changes in the emission current. Heating the tip momentarily, a process known as flashing, can clean it, however new atoms and molecules quickly re-adsorb onto the tip even in the best of vacuums.[41]

Thermally assisted field emission (TFE) sources have an increased stability over FE sources, as they are less susceptible to contamination by gases in the chamber containing the source due to their elevated operating temperature (1800 K and above) These sources typically consist of a tungsten needle that has been sharpened to a point with a radius less than 1 um. They are capable of achieving stable emission currents for months at a time and possess brightness almost as high as the cold FE sources, a very small virtual source size and a moderately small energy spread of emitted electrons Most high-end EBL systems use TFE emitters for these reasons. The only drawback in TFE sources is their inability to achieve the high levels of emission current attainable with thermionic systems [42]

2.1.2 Elements of Electron Optics

Once the electron stream is generated from the source it must be formed into a narrow beam on the order of 5 nm to 10 nm This is accomplished by passing the beam through a series of electrostatic or magnetic lenses and apertures The column will also

contain mechanisms for deflecting the beam and a beam blanker for turning the beam on and off. A stigmator for correcting any astigmatism in the beam, alignment systems for centering the beam in the column, and finally, an electron detector for assisting with focusing and locating alignment marks on the sample constitute the rest of the column components (refer to figure 2-1).[43]

In principle, electron lenses behave the same as optical lenses However, there are some important differences worth noting. With few exceptions, electron lenses can be manufactured only to converge not diverge. Also, the quality of electron lenses is not nearly as good as optical lenses in terms of aberration. There are two types of aberration that seriously effect electron lenses. spherical aberrations, where the outer zones of the lens focus more strongly than the inner zones, and chromatic aberrations, where the electrons of slightly different energies get focussed at different image planes The latter of the two illustrates why a minimal spread in the spectrum of electron energies emitted from the source is desirable. Electrostatic lenses tend to have worse aberrations than magnetic lenses so they are used less frequently in high performance systems.[44]

Apertures are small holes through which the beam passes on its way down the column. Several types of apertures are employed at various stages of the column, each serving a different purpose A spray aperture may be used to stop any stray electrons without materially affecting the beam itself A blanking aperture is used to turn the beam on and off by deflecting the beam away from the aperture hole, intercepting the beam when not writing. A beam-limiting aperture has two effects. it sets the beam convergence angle through which electrons can pass through the system, controlling the

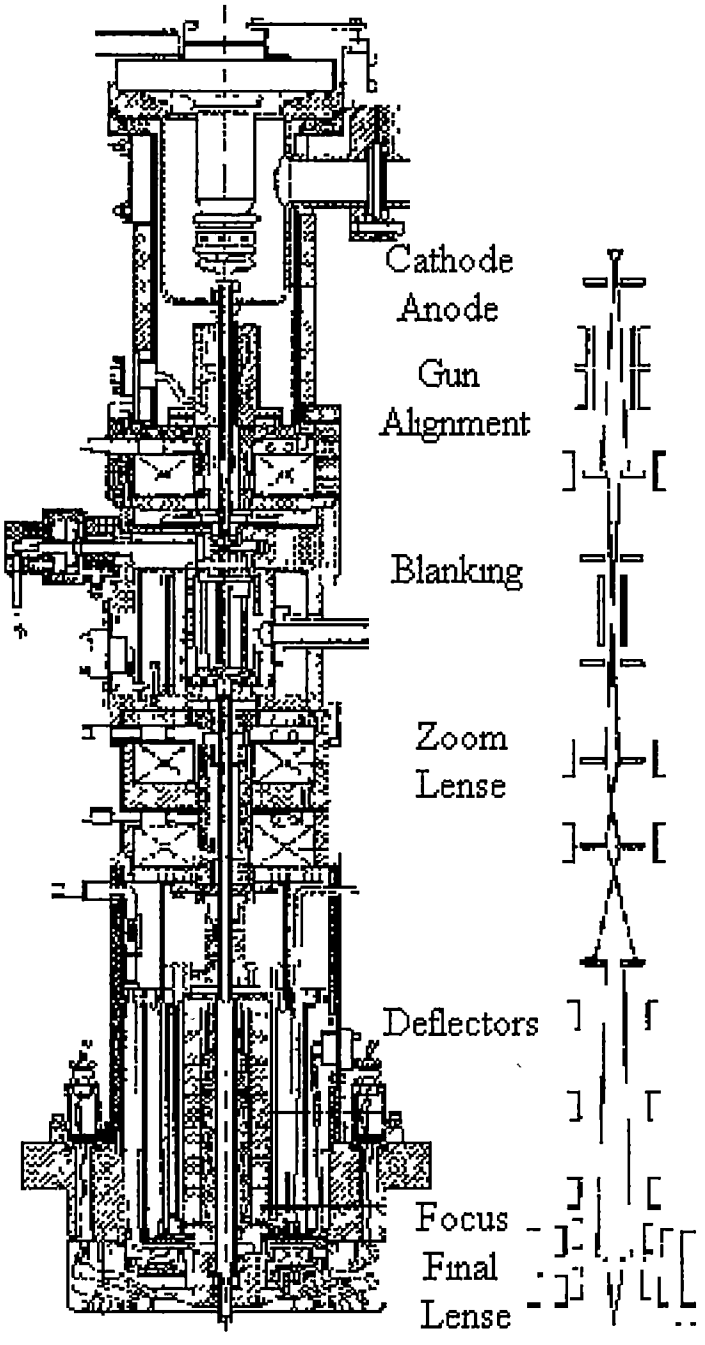

Figure 2-1: Cross-section drawing of a typical electron beam column along with a raytrace of the electrons as they pass through the various electron optical components.[6]

effect of lens aberrations and thus resolution, also this sets the beam current. A beam-limiting aperture is normally set in an X-Y stage to allow it to be centered, or aligned, with respect to the optical axis of the beam Apertures may also be heated to help prevent the formation of contamination deposits, which can degrade the resolution of the systems [45]

Deflection of the electron beam is used to scan the beam across the surface of the substrate without physically moving the stage on which the substrate rests The extent over which the beam can be deflected without degrading its integrity is commonly referred to as the field size As with electron lenses, deflection can be accomplished either magnetically or electrostatically Deflecting the beam off axis introduces additional aberrations that cause the beam diameter to deteriorate, and deviations from the linearity in X and Y increase as the amount of deflection increases These effects combined with the aberrations from the lenses limit the maximum field or deflection size that can be used Some tools introduce dynamic corrections to the deflection, focus and stigmators in order to increase the maximum field size, at the cost of additional system complexity.[46]

The function of the beam blanker is to switch on and off the current in the electron beam This is usually accomplished with a pair of parallel plates set up as a simple electrostatic deflector One or both of the plates are connected to a blanking amplifier with a fast response time. In order to be effective, the blanker must also provide a high degree of beam attenuation in the off state and limit any spurious beam motion induced by the blanking system to a distance much less than the size of a single exposure

pixel.[47] To turn the beam off, a voltage is applied across the two plates which sweeps the beam off axis until it is intercepted by a downstream aperture.[48]

A stigmator is a special type of lens used to compensate for imperfections in the construction and alignment of the EBL column. These imperfections can result in astigmatism, where the beam focuses in different directions at different lens settings; the shape of a nominally round beam becomes elliptical with the direction of the principal axis dependent on the focus setting resulting in smeared images in the resist layer being exposed. The stigmator cancels out the effect of astigmatism, forcing the beam back into its optimum shape. Stigmators may be magnetic or electrostatic and consist of four or more poles arranged around the optical axis. [49]

The final required component of an EBL system is a method of detecting the emitted electrons for focusing, deflection calibration, and alignment mark detection. Usually the detector is a silicon solid-state detector mounted on the end of the final lens just above the sample EBL systems normally detect high-energy backscattered electrons since these electrons can more easily penetrate the resist film The signal from low-energy secondary electrons may be obscured by the resist [50]

2.1.3 Resolution

There are several factors that determine the overall resolution of an EBL system. First is the virtual source size, d_v, divided by the demagnification of the column, M^1, resulting in a beam diameter, d_g If the optics of the column were ideal, this simple

relation would determine the beam diameter. In reality lenses are far from perfect. Spherical aberrations caused by the lenses result in a distortion of the ideal beam diameter, d_s, that can be controlled by using an aperture to limit the convergence angle of the beam. Unfortunately, this results in a somewhat diminished beam current Chromatic aberrations also result in degraded beam diameter, d_c, and are best controlled at the electron source by choosing a source material that provides limited electron energy spread Finally rudimentary quantum physics permits the calculation of the electron wavelength as

$$\lambda = \frac{1\,2}{(V_b)^{\frac{1}{2}}}\text{nm}, \qquad (2\text{-}1)$$

where V_b is the beam voltage. Although this is much smaller than the wavelength of light (008 nm at 25 kV), this wavelength can still limit the beam diameter by classical diffraction effects in very high-resolution systems For a diffraction limited beam, the diameter is given by

$$d_d = \frac{6\lambda}{\alpha}, \qquad (2\text{-}2)$$

where α is the convergence half-angle of the beam at the substrate[51] To determine the theoretical beam spot size of a system, the contributions from various sources of

aberration can be added in quadrature This gives the final spot diameter on the surface of the substrate as

$$d = \left(d_c^2 + d_s^2 + d_g^2 + d_d^2\right)^{\frac{1}{2}} \qquad (2\text{-}3)$$

In systems with thermionic sources, spherical aberrations tend to be the limiting factor for beam diameter, while chromatic aberrations dominate in field emission systems. For a given beam current, there will be an optimum combination of convergence angle and system demagnification Resolution can generally be improved in most systems by using a smaller beam-limiting aperture, at the expense of reduced beam current and throughput In systems where the demagnification can be varied, increasing the demagnification will also improve resolution at the expense of reduced beam current.[52]

2.1.4 Electron Solid Interactions

EBL systems are capable of generating extremely narrow beams, however the interaction of the beam with the substrate being exposed causes changes in the quality of the beam that are difficult to correct for in the column The chief mechanism for these changes is electron scattering events. As the electrons penetrate the resist, they experience many small angle scattering events, commonly referred to as forward scattering, with respect to the incident velocity This can result in a significantly broader

beam profile at the bottom of the resist layer than at the top The increase in effective beam diameter in nanometers due to forward scattering is given empirically by the formula

$$d_f = 9\left(\frac{R_t}{V_b}\right)^{1.5} \text{ nm}, \qquad (2\text{-}4)$$

where R_t is the resist thickness in nanometers and V_b is the beam voltage in kilovolts This shows that using the thinnest possible resist and the highest available accelerating voltage minimizes forward scattering [53]

As the electrons penetrate through the resist into the substrate, they occasionally undergo large angle scattering events, in a process known as backscattering These electrons may return back through the resist at a significant distance from the incident beam, causing additional resist exposure This phenomenon is commonly known as the proximity effect where electrons scattering from other nearby features affect the dose that a pattern feature receives The range of the electrons, defined as the distance a typical electron travels in the bulk material before losing all its energy, depends on both the energy of the primary electrons and the type of substrate For a high energy beam this dispersal may be sufficient to reduce the exposure dose enough to prevent a significant change in the resist properties over the entire area, unless the resist has a very high sensitivity. The fraction of electrons that are backscattered is roughly independent of beam energy, although it does depend on the substrate material with low atomic number

materials giving less backscatter. Using a thin layer of resist can help to minimize backscatter.[54]

As the primary electrons slow down, much of their energy is dissipated in the form of secondary electrons with energies ranging from 2 to 50 eV. They are responsible for the bulk of the actual resist exposure process Since their range in resist is only a few nanometers, they contribute little to the proximity effect. Instead the net result can be considered to be an effective widening of the beam diameter by roughly 10 nm. This largely accounts for the minimum practical resolution of 20 nm observed in the highest resolution electron beam systems and contributes to the bias that is seen in positive resist systems, where the exposed features develop larger than the size they were nominally written. [55]

2.1.5 Proximity Effect Correction

A major concern in EBL is pattern distortion due to proximity effects. Several schemes have been devised to minimize the proximity effect The most common process for proximity effect correction is referred to as dose modulation, where each individual shape in the pattern is assigned a dose such that the shape prints at its correct size. For practical reasons, proximity correction is normally thought of in terms of the large pattern areas receiving a base dose of unity, with the smaller and/or isolated features receiving a larger dose to compensate as necessary. If a pattern has a fairly uniform density and

linewidth, all that may be required is to adjust the overall dose until the patterns come out the proper size.

A similar approach to dose modulation is pattern biasing. In this approach, the extra dose that dense patterns receive is compensated for by slightly reducing their size This technique can be implemented on all EBL systems, however it does not posses the dynamic range that dose modulation has. Patterns that contain isolated features and very dense features will have reduced process latitude compared with dose modulation as the isolated features will be under-dosed and the dense features will be over-dosed Pattern biasing cannot be applied to features with dimensions close to the scale of the scale of the pixel spacing if the EBL system.

Higher beam voltages from 50 kV to 100 kV or more also minimize forward scattering, although in some cases this can increase the backscattering Conversely, by going to very low beam energies, where the electron range is smaller than the minimum feature size, the proximity effect can be eliminated The penalty is that the thickness of a single layer of resist must also be less than the minimum features size so that the electrons can expose the entire film thickness. [56,57]

2.2 EBL Systems

2.2.1 Overview of EBL Systems

Direct write systems can be classified into two general categories: raster scan and vector scan with either a fixed or variable beam geometry. Raster scanning was used in early EBL systems. In a typical system the beam first passes through a pair of blanking plates that can deflect the beam into a beam stop. A second pair of plates is used to scan the beam in one direction while the stage is mechanically scanned in the direction perpendicular to the beam scan Using the raster scan method, every pixel must be scanned serially, and thus the exposure time is nearly independent of the pattern. The pattern is written by opening and closing the shutter

Vector EBL systems have been developed to improve throughput by directing the electron beam to only those parts of the chip to be exposed. In this method the digital location of each area to be exposed is fed to a series of digital to analog converters (DAC). The speed of the DACs is a critical concern in determining system throughput for vector scan systems. The beam is directed only to those pixels so as to minimize the time consumed by beam deflection. By using high-speed DACs with wide words, each pixel can be placed on an extremely fine grid without requiring the beam to access each individual pixel.

A variable shape beam can be produced in either the raster scan or vector scan system by partially intercepting the beam with a square aperture By changing the

deflection the width and length of the line can be varied. Shaping in the x and y directions can be done independently. An electrostatic rotation lens can be added to produce rectangles at random angles This allows hundreds of pixels to be exposed simultaneously [58]

2.2.2 Leica Lithography Systems

The Leica Vector Beam (VB) systems constitute the high end of Leica's EBL systems The VB systems feature a thermal field emission electron source running at 100 kV. The pattern generator (PG) runs at 25 MHz and has a memory buffer capable of storing repeated patterns, eliminating the need to retransmit them to the PG This ability can significantly decrease the transmission overhead time when writing a large array of simple figures Leica EBL tools are distinguished from those of other manufacture by their unique column design and scaleable exposure field size with 2^{16} pixels across the field The VB systems also include a glancing-angle laser height sensor for dynamic focus/astigmation corrections. [59] The Leica VB6 boasts a minimum electron beam diameter less than 5 nm allowing for the exposure of feature sizes less than 20 nm over maximum field sizes of 655 μm on a side. Substrate positioning is monitored by a laser interferometry-based feedback system, capable of locating samples with 0 6 nm of precision. [60]

2.3 Advantages and Disadvantages of EBL

Direct write EBL systems of one form or another have become the standard research tool for device fabrication below 100 nm The literature abounds with uses of EBL to create traditional electronic devices, quantum effect devices, and structures for the study of molecular monolayers and biological systems. This proliferation of EBL processes is largely due to its inherently high resolution and the relative ease with which one can develop an EBL process. EBL does not rely on masks and the range of patterns one can fabricate is diverse. EBL exposures can be used in combination with a variety of pattern transfer techniques and can be performed on a large variety of substrates.

The major shortcoming of EBL is the notoriously long exposure time for large patterns due to the serial nature of EBL systems. Direct write EBL systems offer no means for exposing pattern features in parallel and, unlike photolithography, there is a limit to the number of pixels a beam can expose at any given time This makes the exposure time for EBL systems dependent on the pattern being exposed, rendering it somewhat unpredictable As a consequence, direct write EBL is currently a viable option only for the fabrication of small batches of devices for research purposes and is currently incompatible with commercial fabrication lines requiring wafer throughputs above 50 wafers per hour.[61]

2.4 EBL Resists

Electron sensitive resists are the recording and transfer media for EBL In an optical lithography process, the energy of the absorbing photon is well defined. In contrast, a high concentration of secondary electrons with a wide range of energies is produced on exposure to the electron beam. Rather than designing the resist so that a single chemical reaction is driven by the exposure, an EBL resist must be designed so that the desired reaction occurs preferentially, while recognizing that many reactions will occur

The resists that are often used in EBL consist of long chain carbon polymers dissolved in a liquid solvent Liquid resist is dropped onto the substrate and then spun at 1000 to 6000 rpm to form a uniform coating After baking out the casting solvent, electron beam induced irradiation of the atoms on adjacent chains will cause them to either be dissociated or to bond directly to each other depending on the chemical composure of the resist The former process is known as polymer chain scission, the latter is known as polymer chain cross-linking A material in which chain scission is the dominant reaction during exposure is called a positive resist, as the exposed image is washed away in a given developer solution Highly cross-linked molecules dissolve more slowly in a developer solution and are used as negative tone resists Once the pattern is defined it is then transferred to the substrate through an etching process or by "liftoff" of material. In the liftoff process a material is evaporated from a small source onto the substrate and resist. The resist is then washed away in a solvent such as acetone.

A resist is evaluated on two criteria its contrast and sensitivity for the exposure type and energy. The sensitivity of the resist is defined as the point at which all of the resist layer is removed Ideally, the film thickness would drop abruptly to zero at the minimum dose required for exposure, referred to as the critical dose In practice, the film thickness line drops with a finite slope If D_1 is the largest dose at which no film is lost and if D_2 is the dose at which all of the film is lost then we define the contrast γ of the resist by

$$\gamma = \left[\log_{10}\left(\frac{D_2}{D_1}\right)\right]^{-1}. \qquad (2\text{-}5)$$

A higher contrast resist will usually afford increased flexibility in processing as well as a more vertical sidewall profile. In order to help minimize bias and proximity effects, positive resists will usually be exposed and/or developed as lightly as possible while still adequately clearing the resist down to the substrate for all features A brief dry etching or reactive ion etch (RIE) step using an oxygen plasma following developing can assist in removing undeveloped resist from the patterned area without significantly bloating the feature size In EBL, at elevated operating voltages of 50 kV or more, it is possible to make resist structures with very high aspect ratios However, when the aspect ratio exceeds roughly 5:1, most resists undergo mechanical failure during development, due primarily to surface tension in the rinse portion of the development sequence.[62]

The highest resolution resists are usually the least sensitive. This can be explained when the limit of resist sensitivity is considered If a very sensitive resist has a

critical dose of .1 μC/cm^2 and a single pixel is .1 μm on a side, then only 62 electrons are needed to expose the pixel. At this sensitivity, even small changes in the number of electrons will cause variations in the dose delivered to each pixel Decreasing the pixel size will force the resist to be made less sensitive in order to avoid statistical variation in the exposure

2.4.1 Polymethyl Methacrylate

Polymethyl methacrylate (PMMA) was one of the first materials developed for use as an EBL resist. It is the standard positive resist and remains one of the highest resolution resists available PMMA is usually purchased in two molecular weight (MW) forms (496K or 950K) solubalized in a casting solvent such as chlorobenzene or anisole. The casting solvent can be cured at 170°C by baking for 15min to an hour. In PMMA both cross-linking and polymer chain scission occur however, electron beam exposure induces scission at a much faster rate Exposed areas can be dissolved preferentially by a developer such as methyl isobutyl ketone (MIBK). MIBK alone is too strong a developer and removes portions of the unexposed resist. Consequently it is usually diluted by mixing in a weaker developer such as isopropanol (IPA). A mixture of 1 part MIBK to three parts IPA produces a very high contrast but low sensitivity developer By making the developer stronger, for example 1·1, the sensitivity is improved significantly with only a small loss of contrast [63]

2.5 Liftoff Pattern Transfer

Liftoff pattern transfer is arguably the simplest means of transferring the image of an exposed pattern to the substrate. It involves no etching steps, requires only solvents and an agitation source and can be very high resolution In liftoff processes a layer of resist much thicker than the metal layer being deposited is spun and patterned Next a thin layer of metal is deposited using a physical vapor deposition technique Thermal or electron gun evaporation is typically chosen because it deposits a non-conformal film unable to cover step edges of materials, unlike sputtering. If a re-entrant profile is obtained in the resist, a break in the metal is virtually assured. The wafer is then immersed in a solution capable of dissolving the resist The metal lines that were deposited directly on the substrate remain, while the metal deposited onto the resist lifts off of the wafer as the resist dissolves Etch damage to the substrate is avoided and the lines patterned with infinite selectivity with no undercut.[64]

Different methods have been demonstrated for obtaining re-entrant profiles in resist. Most commonly used is the bilayer resist technique that relies on the use of resists that have similar exposure characteristics but different development characteristics. One simple way of achieving this is by using a bilayer of PMMA with different molecular weights (refer to figure 2-2) The choice of a lower molecular weight on the bottom layer with a higher molecular weight on top has been shown to be successful in the production of ~10 nm features. The lower molecular weight will develop faster than the higher molecular weight leaving the desired re-entrant profile

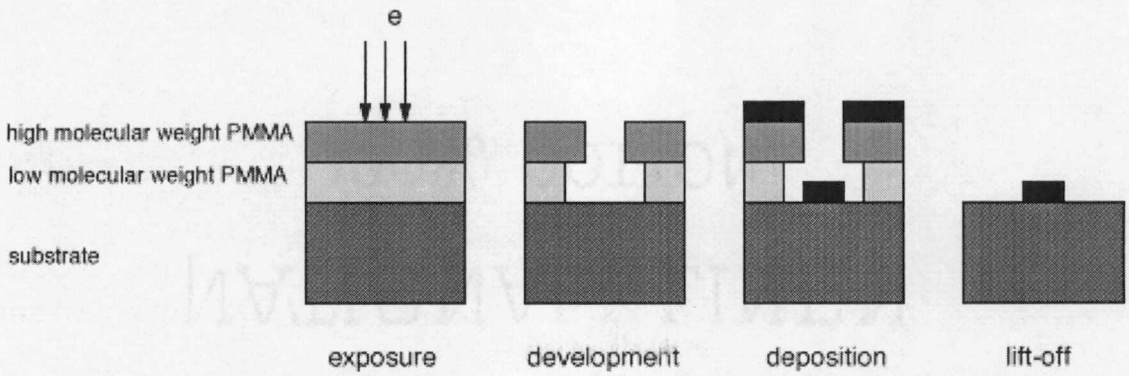

Figure 2-2: Overview of the bilayer resist process for PMMA[65]

2.5.1 Disadvantages of Liftoff Pattern Transfer

Liftoff processes do have several shortcomings that make them disadvantageous in certain applications The first is that the surface topography must be very smooth, since the metal deposition step is designed to have poor step coverage. The technology therefore, must either be limited to one layer of metallization or each layer must be planarized before liftoff patterning This effectively prevents the use of sputtering as a deposition technique as it has excellent step coverage. The most serious problem with liftoff is that the metal lifted off is retained in solid form and floats in the bath. Pieces are very likely to deposit on the surface of the wafer accidentally Unless the patterns are very simple, liftoff can have serious yield impacts.[66]

Chapter 3

Design of the DiMEND Structures

3.1 Background

The issues involved with fabricating electrode pairs suitable for the electrical characterization of molecular junctions were discussed in chapter 1. In this discourse the Photosystem I (PSI) reaction center was used as an example of a molecule with orientation dependent electrical properties. These properties render the incorporation of the PSI into metal/PSI/metal heterojunctions somewhat difficult when that metal on each side of the junction is of the same material. It was also mentioned that if electrode pairs could be fabricated of dissimilar metals that this problem could perhaps be eliminated. In order to gain a deeper understanding of how this capability will facilitate the electrical characterization of molecules with orientation dependent electrical properties, the properties of the PSI reaction center will be examined The self-assembly techniques that have been developed to control its orientation with respect to Au substrates will also be discussed A brief review of self-assembly based metallic surface modification techniques will be given followed by a detailed description of the design of the DiMEND structures

3.1.1 Structure of the Photosystem I Reaction Center

The photosynthetic apparatus in green plants and algae is contained in a unique cellular organelle known as the chloroplast. A double membrane composed primarily of thylakoids encloses the chloroplast The thylakoids contain stacked membrane disks (grana) and unstacked membrane disks (stromal regions) Photosystem I (PSI) reaction centers are embedded in the thylakoid membrane. These molecules are responsible for driving the light dependent transfer of electrons from plastocyanin (a copper containing soluble protein located in the luminal space of the chloroplast thylakoids) to ferredoxin (a [Fe-2S]-containing soluble protein located in the chloroplast stroma) [67]

The PSI reaction center has been measured by electron microscopy to be 10nm x 15 nm, or 7 nm x 12 nm after correction for attached detergent used to stain the molecules.[68] It has been shown that platinum can be precipitated on the surface of photosynthetic membranes, thereby making direct electrical contact with the acceptor side of the PSI[69], where it can either catalyze hydrogen evolution or drive photocurrent through an external circuit [70] It was also demonstrated that PSI reaction centers can be platanized without altering their intrinsic photo-excitation dynamics and initial electron transfer reactions.[71]

3.1.2 Preferential orientation of the PSI and Electrical Characteristics

The attachment of platinum to the acceptor side of the PSI has been shown to significantly affect its electrical properties. This can be observed by a sustained steady-state vectorial flow of current through the molecule Using scanning tunneling spectroscopy (STS) a band-gap was clearly seen in unmetallized PSI while platinized PSI was shown to have a current rectification property analogous to a semiconductor PN-junction diode [72] The exact mechanism for these electrical properties is not known. The PSI reaction center has an oxidizing potential of about +.4 V at the electron donor side and a reducing potential of about - 7 V at the acceptor side[73] The asymmetry of the I-V curve may be due to either a difference in electronic energy or a difference in the tunneling distance for each end.

Thiol-based molecular self assembly techniques have been employed to anchor two dimensional arrays of PSI onto a Au{111} substrate and obtain controllable orientation. Gold substrates immersed in 10 mM solution of mercaptoacetic acid, 2-dimethylaminoethanethiol or 2-mercaptoethanol for 30 s to form a negative, positive or hydrophilic surface, respectively have been studied Following incubation in PSI solution for 12h the coverage of PSI molecules on each substrate was analyzed with both atomic force microscopy (AFM) and STM and found to be highly dependent on the modification performed on the Au surface [74]

The coverage of three 1 μm x 1μm areas were examined on each type of modified Au substrate and then averaged. The Au surface treated with mercaptoacetic acid was

shown to be covered 65 ± 7 % with PSI. This chemical treatment was designed to terminate the Au surface with negatively charged end groups that could attract and orient the PSI. Previous studies have shown that the polar regions (both ends) of the PSI are positively charged[75]. Very little PSI coverage was found on the 2-dimethylamino-ethanethiol, 5 ± .7 %. This treatment effectively terminated the surface with positively charged end groups Substrates treated with the 2-mercaptoehtanol were found to have an average coverage of 70 ± 11 % with PSI. This treatment was used to terminate the surface of the Au with end groups that form H-bonds with PSI [76]

Scanning tunneling spectroscopy techniques[77] were employed to determine the orientation of the PSI on the chemically modified Au substrates detailed above. STS was performed on 100 individual PSI reaction centers in a 200 nm x 200 nm area on each of the three types of substrates. If a PSI is oriented with its electron transport vector (ETV) parallel to the substrate surface a semiconductor-like I-V curve with a band gap of ~1 8 eV can be observed. If a PSI is anchored with its ETV perpendicular to the gold surface a diode-like current rectification I-V curve can be observed. Note that the orientation of the PSI is described as "up" if the ETV is oriented from the substrate to the STM Tip and "down" if the ETV is oriented from the STM tip to the substrate The results of these experiments are shown in Table 3-1[78]. From this data it was concluded that 2-Mercaptoethanol is capable of orienting the PSI in an up position on the Au substrate while Mercaptoacetic acid is capable of orienting PSI in a parallel position with respect to the substrate.

Table 3-1: Orientation Statistics of the PSI on Treated Au Surfaces

Surface treatment	Up (%)	Parallel (%)	Down (%)
Mercaptoacetic Acid	9	83.1	7.9
2-Dimethylaminoethanethiol	31.2	32.7	36.1
2-Mercaptoethanol	70 1	28.4	1.5

estimated error· 10%

3.2 The DiMEND Structures

3.2.1 Self Assembled Monolayers on Metallic Substrates

It is clear from the research performed on preferentially orienting PSI on flat Au substrates that alkane-thiol self assembled monolayers (SAM) can be used to control the deposition of PSI onto Au structures Alkane-thiols on Au are one of the most widely studied SAM systems discussed in the literature. A significant amount of research has also been done on SAM coverage of non-Au metallic substrates [79] This body of work has shown that thiol-based SAMs, while being very effective on Au[80], Pt[81], Ag[82] and Cu[83] substrates, exhibit poor coverage on metals that produce an oxide[84], such as Ti and Al. It has also been shown that nitrile based SAMs are effective in covering Pt while showing little preference for Au [85] Once covered, these modified Pt substrates show almost no affinity for the thiol-based SAMs.

Using the data on SAM coverage of metallic substrates presented in the literature, dissimilar metal electrodes with nanometer interelectrode distance (DiMEND) were designed to electrically characterize the PSI molecule These electrode pairs contained one Au electrode that could be used to control the deposition and orientation of the PSI by covering it with a 2-mercaptoethanol SAM. The material of the second electrode was chosen such that it would either be unaffected by the 2-mercaptoethanol SAM or be capable of being chemically altered to resist coverage by thiol-based SAMs (refer to figure 3-1).

3.2.2 Bulk PSI Measurement Structure

The first DiMEND structure was designed to examine the electrical properties of a bulk sample of oriented PSI reaction centers. These structures consisted of a dissimilar metal electrode pair with T-shaped tips extending 300 μm wide and separated by a distance suitable for making direct contact to the PSI These electrodes were each connected to a 250 μm x 250 μm probing/wire-bonding pad to facilitate electrical characterization and packaging of these structures (refer to figure 3-2)

As stated previously, one of the electrodes on each of the designed structure was fabricated of Au, providing a mechanism for using the 2-mercaptoethanol to control the deposition and orientation of the PSI In theory, the step edge of the Au electrode tip should provide enough surface area for the PSI to self-assemble onto the 2-mercapto-ethanol SAM By depositing a layer of Au 30 nm thick the surface area of the electrode

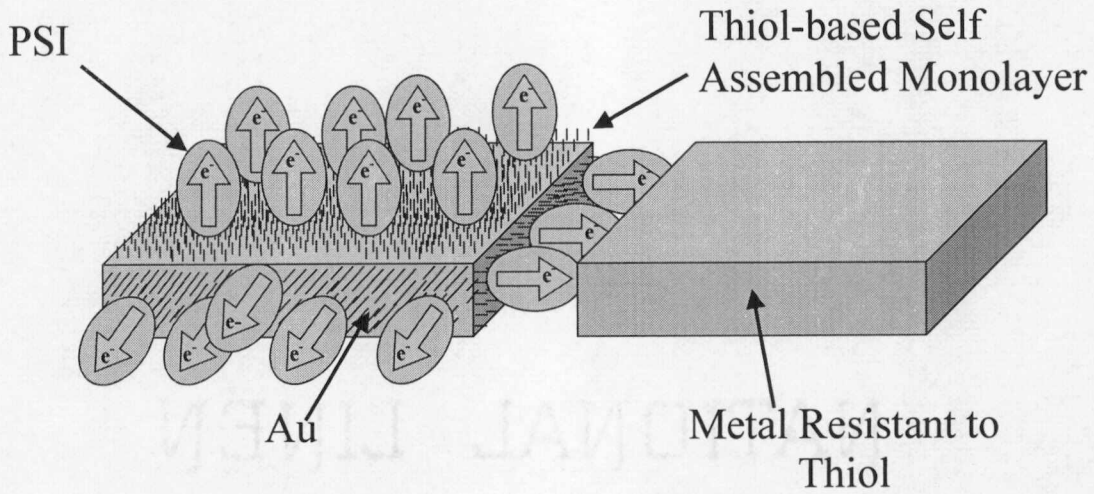

Figure 3-1: Diagram of PSI self-assembled with thiol-based SAM to Au electrode in a DiMEND structure

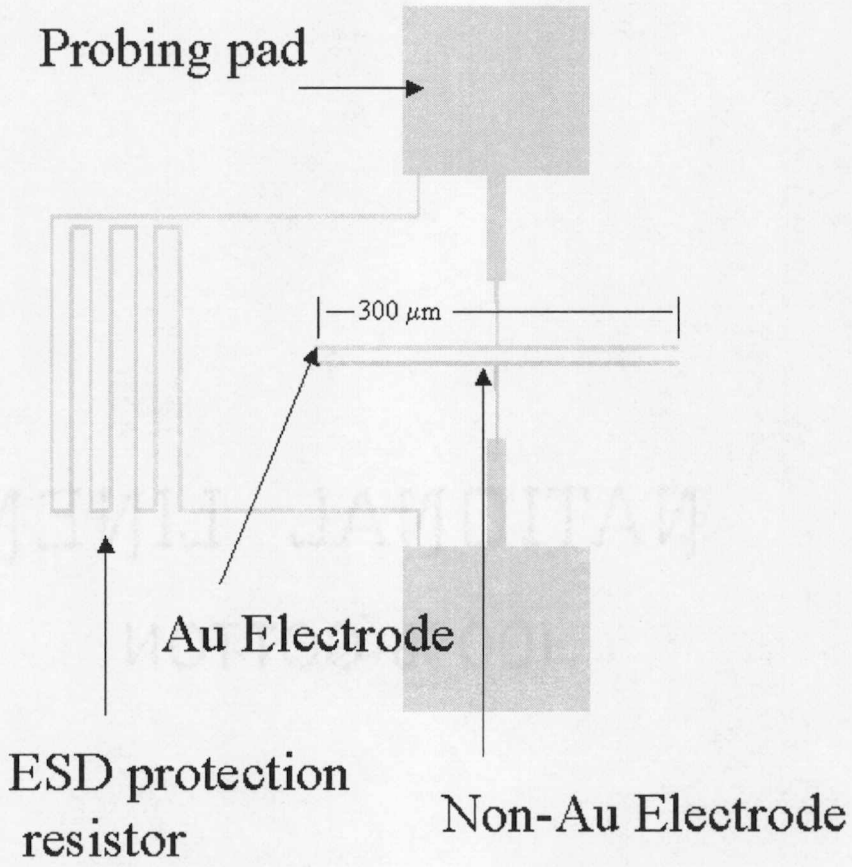

Figure 3-2: Diagram of the designed bulk PSI measurement structure

tip should be 9 μm^2. Assuming that there would be at least 100 PSI reaction centers in a 200 nm x 200 nm area, the possibility of having $2.25x10^4$ reaction centers in parallel is created.

The ideal interelectrode distance for making direct contact to the PSI is on the order of 10 nm. The electric field developed across this gap by electrostatic discharge could potentially destroy the electrode structure. In order to minimize the risk presented by ESD a resistor was incorporated into the structure design, connecting the two bonding pads together Before making a measurement this resistive path can be opened by severing its connection to one of the pads with a diamond scribe

3.2.3 Single PSI Measurement Structure

The second DiMEND structure was designed to measure the electrical properties of a limited number of PSI reaction centers. This structure was designed to have rectangular tip geometry with a tip width of 50 nm and an interelectrode distance suitable for contacting both ends of the PSI By choosing the material of one of the electrodes to be Au, the use of 2-mercaptoethanol should allow preferential deposition and orientation of the PSI Using a 30 nm thick layer of Au and assuming that there are at least 100 PSI in a 200 nm x 200 nm area, as few as 4 PSI could potentially be present in the interelectrode gap. The same bonding/probing pad and ESD protection resistor scheme presented for the bulk PSI measurement structure were used in this structure (refer to figure 3-3).

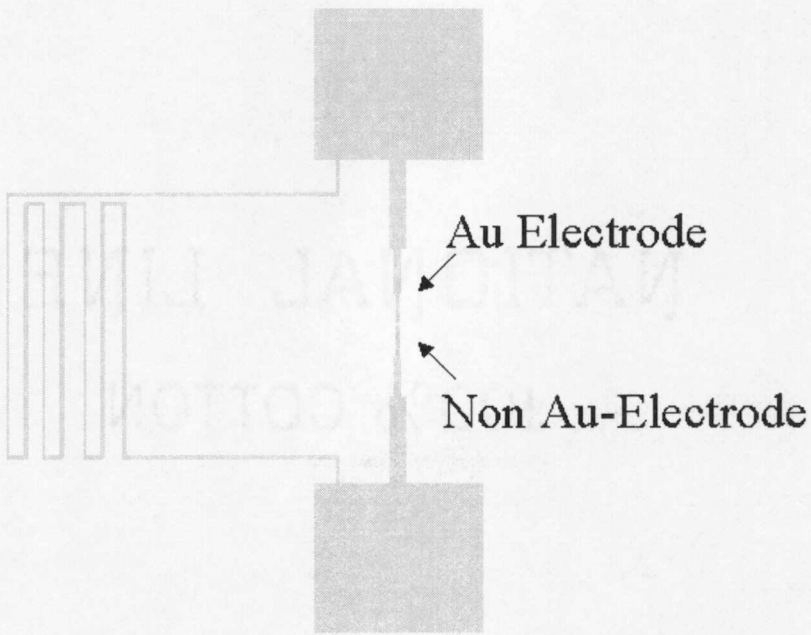

Figure 3-3: Diagram of the designed single PSI measurement structure

3.2.4 Four Terminal PSI Measurement Structure

The third and final DiMEND structure was designed to demonstrate the possibility of employing the current rectification properties of the PSI reaction center to realize a Boolean logic function via diode-resistor logic This was to be accomplished by fabricating a Au electrode and at least two other dissimilar metal electrodes within an interelectrode distance suitable for making electrical contact to the PSI.

In the designed structure three dissimilar metal electrodes surrounded the tip of the Au electrode in a cross-like fashion (refer to figure 3-4). Three electrodes were used instead of two to maximize the probability of successfully realizing the desired electrical configuration. The geometry of the electrodes was identical to that of the single PSI measurement structure, creating the same surface area restrictions thus limiting the number of active PSI reaction centers involved in a working device.

The ESD protection scheme for this structure differed slightly from that of the other two DiMEND structures in that it was necessary to couple all four terminals This was realized by placing a resistor between each of the pads forming a conductive ring around the structure

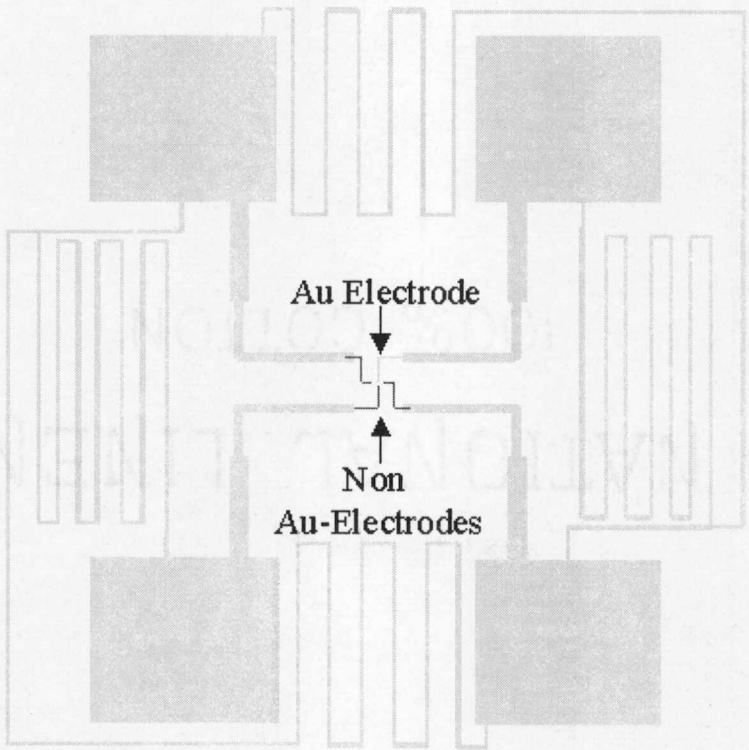

Figure 3-4: Diagram of the designed four terminal PSI measurement structure.

Chapter 4

Fabrication of the DiMEND Structures: Methods and Materials

4.1 Overview of the DiMEND Process

The DiMEND fabrication process involves several successive direct-write EBL and PVD metallization steps. An overview of the process flow for a single patterning and metallization step is provided in figure 4-1 It should be noted that this process does not rely on any novel or unique processing techniques beyond the high resolution EBL patterning, which is fairly standard.

4.2 Sample Preparation

The substrates used throughout this work were 3" p-type Boron doped Si <100> wafers with a resistivity of 10-20 Ωcm These wafers were passivated with 2000 Å of thermally grown SiO_2. Prior to any processing, an initial inspection of the quality of the oxide was performed using an optical microscope After ensuring that the oxide was relatively free of gross defects, the wafers were immersed in an acetone (ACE) bath and placed in an ultrasonic cleaner for 2 minutes After this cleaning, the wafers were removed from the bath and rinsed in isopropanol (IPA) and blown dry with a high-pressure jet of dry, filtered N_2.

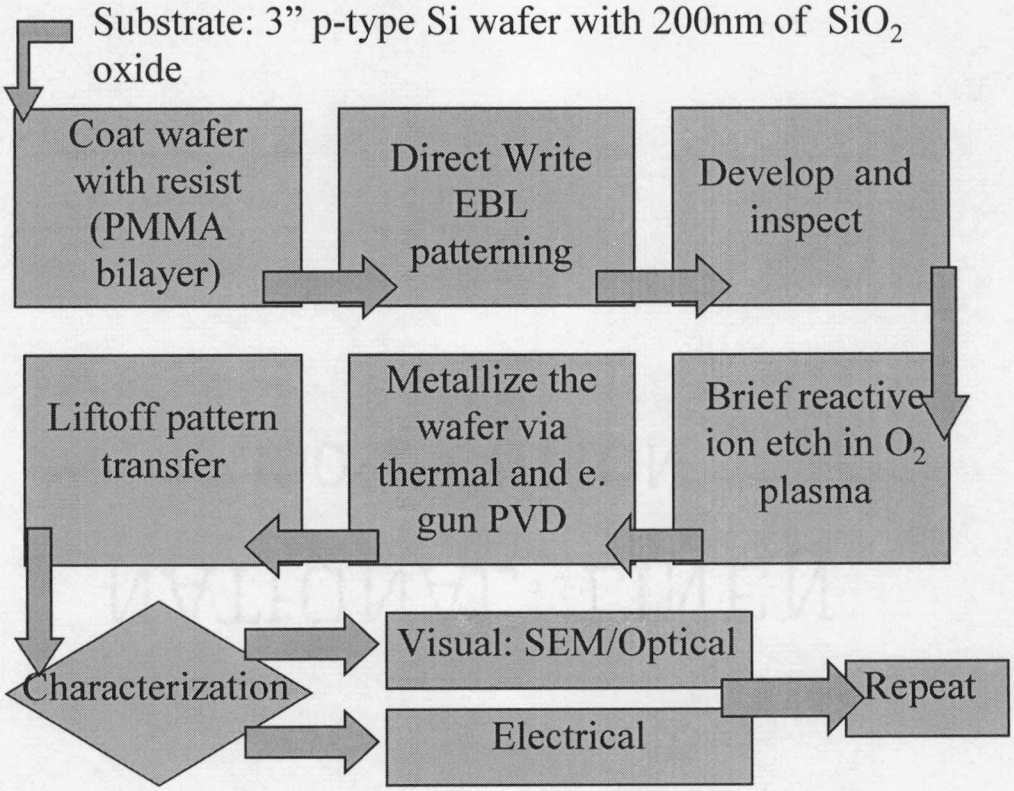

Figure 4-1: Diagram of the process flow for a single EBL patterning and metallization step.

4.3 Resist Process

A bilayer of poly(methyl methacrylate) (PMMA) was used as the electron sensitive resist in this process. The lower layer of PMMA consisted of 2% 496K PMMA in chlorobenzene, the upper of 2% 950K PMMA in methyl isobutyl ketone (MIBK) Each layer was spun onto the wafer at a speed of 2000 rpm for 60 s to provide layers of roughly 800 Å thickness For each resist layer, approximately 0 2 ml of PMMA was deposited onto the center of the wafer followed by immediate activation of the spin coater. This is a well-established protocol for generating coatings of uniform thickness Disposable plastic pipettes were used to deposit the resist onto the wafers Each pipette was blown clean with dry N_2 to avoid contaminating the resist layers with foreign particles After each coating step the wafers were baked on a 170 °C hotplate for 15 minutes in filtered room air to cure the casting solvent Great care was taken to achieve particle free coatings of resist for both layers Wafers that showed any evidence of uneven layers due to surface contaminants (dust, hairs, fibers, etc.) or poor spinning practice were stripped clean and processed again until an acceptable bilayer coating had been achieved

4.4 Alignment Level

4.4.1 Patterning of the Alignment Level

Following the resist coating process, wafers were blown clean with dry N_2 placed into the 3" wafer cassette for the VB6 and loaded into the machine for the first level of patterning. At this time the electron beam current was programmed on the VB6 by loading the desired value from a current database file. This file contained the parameters required by the electron column to achieve the desired value of current. For the alignment level patterning step a value of 12 nA was used with a pixel size of 20 nm. After allowing the VB6 to adjust to this current, the current was verified by measuring it with a faraday cup located inside the column. Exposures were performed at a fixed dose of 800 $\mu C/cm^2$.

This layer consisted of a grid of alignment mark patterns spaced by 5 mm in both the x and y directions. Initially arrays of 11x11 were patterned on the wafers. However, it was found that using a grid of this size and pitch resulted in patterning defects in the die present at each corner of the array. These defects were caused by the VB6 attempting to write features beyond the physical boundary of the wafer. As a consequence 10x10 arrays were used for the bulk of the wafers processed in this work.

The alignment mark pattern consisted of a set of twelve 10 μm wide octagons and eight 4 um wide, 300 μm long rectangular lines arranged as shown in figure 4.2. The rectangles and the outer most set of four octagons constituted the wafer level alignment marks on

each die The location of the octagons with respect to the center of the alignment mark pattern is shown in figure 4.2 These octagons were used to remap the coordinate system of the VB6 onto the coordinate system of the wafer before each exposure The rectangular lines were used to facilitate the process of locating the octagons in the optical and electron microscopes used in the alignment process. The other eight octagons were contained within a single 300 μm wide square centered about the relative origin of each die. The centers of these octagons were placed at the points of two concentric squares with sides of 125 μm and 100 μm centered at the origin These marks were used to accurately align exposures within a single 300 μm by 300 μm field, referred to as the fine field Four marks were used per registered exposure in the fine field For the DiMEND process two registered exposures in the fine field were required giving the need for eight octagonal marks.

The first layer of patterning required no registration to pre-existing features on the wafer This type of lithography step is referred to as an unregisterd exposure, one where the VB6 is not aligning to a predefined pattern. The pattern written in this first layer served this purpose in all subsequent exposures. For unregistered exposures the VB6 maps the center of the wafer to a relative coordinate position of 0,0 on a Cartesian plane. It then moves or "steps" to each specified location and exposes the given pattern without realigning For the 10x10 arrays, of devices the starting position of the array was given as (-22 5 mm, -22 5 mm) to produce a symmetric distribution of die across the wafer.

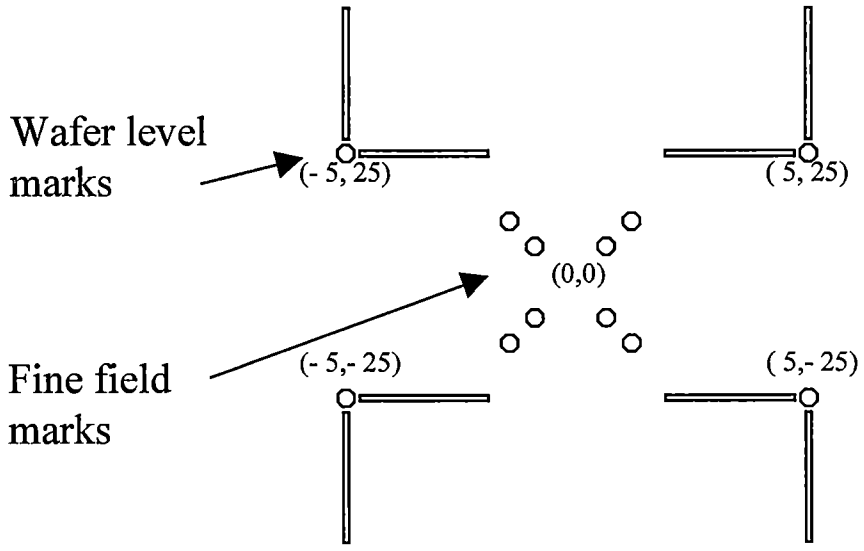

Figure 4 2· Diagram of the alignment mark layout used in the EBL patterning steps showing the relative position of the four wafer level marks to the center of the die The centers of the eight octagons in the fine field are contained on two concentric squares centered at the origin. The outer four are contained on a square with 125 μm sides; the inner four are contained on a square with 100 μm sides

4.4.2 Development of the Alignment Level

Following the alignment level patterning, the wafers were removed from the VB6 and placed into clean fluoroware containers. All exposures were developed in a solution of IPA MIBK 3 1 for 1 minute, rinsed thoroughly in IPA to dilute residual traces of MIBK and then blown dry in a jet of N_2 This relatively weak mixture of developer is typically used in processes with deep submicron features as it affords a tighter degree of control over the development process

The developed exposures were then inspected with an optical microscope The definition of the patterns was observed and the quality of the development was judged. Often when using a weak developer, features will not develop completely in an exposed area, leaving a residue on the order of 10 Å of undeveloped PMMA inside the developed pattern area Failure to remove this layer can result in adhesion problems during pattern metallization, and electrically shorted or opened metal traces. Removal of this layer was performed using a brief reactive ion etch (RIE) step, commonly referred to as descumming In this process an O_2 plasma is used to anisotropicaly etch the undeveloped resist layer from the exposed pattern area without grossly affecting the pattern definition The oxygen flow into the chamber was fixed at a rate of 30 sccm at a chamber pressure of 10 miliTorr, a plasma power of 0 25 W/cm^2 was used. Depending on the quality of the developed resist etch times between 6 s and 10 s were used

4.4.3 Metallization of the Alignment Level

Following the RIE step the wafers were then inspected with an optical microscope to judge the effectiveness of the descum process If no traces of residual resist could be identified at 1000x magnification the wafers were blown clean with dry N_2 to remove any surface contaminants and then loaded into a physical vapor deposition system

The alignment system of the VB6 uses a backscattered electron detector mounted in the objective lens of the electron gun system For this reason, a reasonably thick layer of Au is desired for alignment mark metallization to insure a high contrast, high definition set of marks A 50 Å layer of Cr was thermally evaporated at a rate of 5 Å/s onto the wafer to provide a strong adhesion layer between the SiO_2 surface and the Au layer. 950 Å of Au was then deposited thermally at a rate of 10 Å/s Samples were allowed to cool for five minutes in vacuum following the final film deposition and then removed from the evaporator chamber.

Metallized substrates were then placed in a solution of ACE·Methylene Chloride 1 1 Both of these solvents serve to dissolve the layer of unexposed PMMA and in effect remove the metal layer deposited on the unexposed areas of the wafer The metal deposited into the exposed areas of the pattern is bonded to the substrate material and remains relatively unaffected by this process After a soak in this solution for roughly 1 hr, the beaker containing the solution and the wafer was moved to an ultrasonic cleaner. Ultrasonic agitation was applied for 30 s

Following removal from the ultrasonic bath, the wafer should be free from most of the unwanted metal and PMMA, leaving behind metal only in the patterned areas The wafer was carefully removed from this solution while being continuously rinsed with a jet of fresh ACE Great care was taken to ensure that no pieces of metal from the bath remained on the wafer; unwanted metal can detract from process yield by effectively depositing metal at random locations on the wafer While rinsing with ACE, the wafer was transferred to a fresh beaker of ACE. At this time the wafer was either left for a longer amount of time to soak or it was placed into the ultrasonic cleaner If ultrasonic cleaning was repeated, it was done so for 30 s or less The wafer was then removed from the beaker while being rinsed with IPA, again making certain that no stray metallic debris were present on the surface of the wafer A high-pressure N_2 jet was then used to blow the wafer dry The wafer was placed into its fluoroware receptacle until metrology could be performed

Examination of the alignment level metallization was performed with an optical microscope, as the pattern features did not fall below 1 μm. The quality of the metal was inspected while scanning for the presence of metal debris from the liftoff process or from damaged areas of the resist.

4.5 The First Registered Layer

The first registered exposure performed in the DiMEND process originally included two exposures at different beam currents in the same layer of resist that would

both be developed at the same time and metallized with Au. These two exposures can be broken down into the coarse features (bonding pads, macroscopic leads and the ESD protection resistor) and the fine features (the Au electrode of the DiMEND) This was done to enhance process throughput It was found however that this approach created problems with the integrity of the second electrode as will be discussed in Chapter 5. Consequently these two patterning steps were split into separate events in subsequent process runs. The bulk of the structures fabricated in this work were done so by combining these two exposures into a single level of patterning This chapter will discuss the DiMEND process using this method. The changes to the exposure process will be discussed in Chapter 5

4.5.1 Patterning of the First Registered Layer: Coarse Features

Prior to resist coating, the wafer was placed onto the spin coater chuck. The spinner was then engaged, but resist was not applied at this time Instead, streams of ACE and then IPA were used to clean the wafer while it was revolving and then left to spin dry. This is a proven method for cleaning the wafer surface without using additional ultrasonic agitation, which can damage submicron metallization on the wafer

The wafer was then coated with the same bilayer resist technique described in 4.2, blown clean with N_2, and then placed into the 3" wafer cassette The cassette was mounted on a microscope with a precision xy locator stage A reference mark on the cassette composed of a 10 μm diameter circle, referred to as circle1, was located and then

mapped to the position 0,0 by resetting the value of the stage location indicator. From this location the lower left octagon in the lower left alignment mark in the grid of alignment marks on the wafer was located manually. This mark was referred to as focus mark 1 (FM1). The relative position to circle1 from FM1 was recorded and the locator was set back to 0,0.

By design, the center of the wafer is located at (23 mm, 22.75 mm) relative to FM1. Using the manual stage controls, the center of the wafer was located and the location indicator was reset to zero The upper left octagon in the upper left alignment mark, referred to as FM2, was located and its position relative to the center of the wafer was recorded, this process was repeated for the upper right octagon in the upper right mark, referred to as FM3. The wafer was then blown clean with a jet of N_2 while remaining in the cassette to minimize any debris present on the surface of the resist coating The cassette was then loaded into the VB6

The integrated scanning electron microscope (ISEM) system on the VB6 was used to locate the circle1 reference mark located on the cassette By moving the stage of the VB6 relative to circle1, FM1 was located. A file created to align the VB6 to prepatterned alignment marks on the wafer was then used to map the coordinate system of the stage onto the coordinate system of the wafer This file requires inputting the locations of the marks found in the optical locator microscope It then used the ISEM to locate the marks and automatically adjust the coordinate system of the stage until the error between the anticipated location of the given alignment mark and the actual location of the mark was minimized At the completion of this file a calibration of the VB6,

referred to as a jobcal, was performed. This procedure ran a diagnostic of the column and then adjusts various elements of the electron optical system until the specified operating point is obtained. Once this was completed the file which controls the exposure, referred to as a job file, was run

In this exposure the pattern for the bonding pads, macroscopic leads and the ESD protection resistor was written For this exposure, identical values for the beam current and pixel size to those given in 4 2.1 were used A dose of 850 $\mu C/cm^2$ was used for the bonding pads and macroscopic leads while a dose of 1500 $\mu C/cm^2$ was used in the exposure of the ESD protection resistor

4.5.2 Patterning of the First Registered Layer: Fine Features

After the exposure was completed, the beam current was then lowered to 1.7 nA and the pixel size was set to 5 nm for fine feature patterning The VB6 was then realigned to the same set of marks used for the coarse feature patterning to eliminate any errors caused during the stage travel in the coarse exposure Following this alignment, another jobcal was performed with the new value of the beam current Upon completion of the jobcal, the job file for the exposure of the fine Au lead was performed A dose of 2000 $\mu C/cm^2$ was used in this exposure. Following the exposure, the cassette was removed from the VB6 and the patterned wafer was removed from the cassette.

The wafer was developed using the same process described previously in 4.2.2 The pattern was inspected with an optical microscope and a descum was performed as

needed. The wafer was blown clean with dry N_2 and placed into a CVC SC4500 physical vapor deposition system. This piece of equipment was designed to facilitate the deposition of metals for liftoff processing. It is capable of thermally evaporating material from one of three resistive heating sources that can be positioned inside the deposition chamber to be located directly underneath the substrate holder This eliminates the problems known as "shadowing" which can occur when the resist sidewall profiles act like physical evaporation masks. The SC4500 also has an electron gun evaporation system with a four source holder, further extending the range of materials that this system is capable of depositing

The final feature of the SC4500 worth noting is the position of its deposition rate monitor. This device is located below the shutter that blocks the wafer from the evaporation source which allows the deposition rate of the evaporated material to be established before the shutter is opened. The evaporation rate effects the grain size of a deposited thin film When metallizing patterns with features less than 100 nm with materials such as Au, which has an inherently large grain structure, it is necessary to control this rate prior to opening the shutter. The ability to realize these deep submicron features accurately is somewhat dependent on this

For the Au metallization, 75 Å of Cr was thermally evaporated at 5 Å/s using a Cr rod source. Following this, 300 Å of Au was thermally evaporated at 10 Å/s using resistive heating of a tungsten boat After this metallization was completed, the wafer was allowed to cool inside the vacuum chamber for 5 minutes prior to venting. The sample was then transferred into a beaker containing a solution of Methylene

Chloride.ACE, 1:1. The sample was left to soak for at least an hour and then a liftoff of the deposited material was performed as described previously 4 2.3.

An optical inspection of the large features was carried out using an optical microscope. The probing pads, resistor and wide Au leads were inspected for damage at random points across the wafer. The sample was examined using a LEO 982 scanning electron microscope (SEM). After sampling random die on the wafer and judging the adhesion of the fine Au electrodes the sample was subjected to a brief descum process to remove any surface contamination generated during the SEM imaging. The value of the ESD protect resistor was also measured at this time using a Karl Suss manual probe station and Keithley source measurement units (SMU).

4.6 Patterning of the Second Registered Layer

Following this cleaning, the sample was coated with a bilayer of PMMA as described above After completing the resist coating process, the substrate was placed into the 3" wafer cassette and loaded onto the alignment microscope Alignment marks were identified in a similar manner as described previously The location of the upper right octagon in the lower left alignment mark, the lower left octagon on the upper left alignment mark and the lower right octagon on the upper right alignment mark were used in this process. The sample was then blown off thoroughly with dry N_2 and the cassette was then loaded into the VB6

After locating the necessary alignment mark on the cassette and executing the alignment file for the second metal electrode exposure, the jobcal was performed and the pattern was exposed using the same beam current, pixel size and dose described previously for the fine geometry Au electrode patterning. The values of the beam current before and after the exposure were recorded. Following the exposure the sample was removed from the VB6, removed from the cassette, developed and descummed as described previously in this chapter. Metallization of the second non-Au electrode was performed using techniques similar to those described previously The second metals included electron gun evaporated Pt, Pd and Ti and thermally evaporated Al. For Pt and Pd deposition, a 275 Å layer of the respective metal is deposited onto a 75 Å adhesion layer of Cr. Ti and Al were deposited directly onto the substrates in 350 Å layers without an adhesion layer.

4.7 Post Processing of the DiMEND Structures: Metrology

The finished structures were then examined in the LEO 982 SEM. After calibrating the measurement feature of the SEM to a grating with a 200 nm period, critical measurements of the interelectrode distances were measured and recorded across the wafer Further metrology of the electrode topology was carried out by atomic force microscopy (AFM) using a Digital Instruments Multimode AFM in the tapping mode

Chapter 5

Results and Discussion

5.1 Bulk Measurement DiMEND

The ideal interelectrode distance for characterizing the bulk electro-optical and electrical properties of the PSI was unknown at the time of structure fabrication As a consequence this distance was varied over a range from 10 nm to 50 nm by incrementally changing the placement of the non-Au electrode between 40 nm to 90 nm with respect to the Au line during patterning The reduction in interelectrode distance seen between the specified pattern and the physically realized structure is a result of proximity effect and bloating of the patterned resist as a consequence of the RIE steps Wafers with 11x11 arrays of devices were written such that the interelectrode distance changed from column to column of every row where an entire column was patterned to have the same dimensions. Figure 5-1 shows an example of the smallest interelectrode distance of this structure that could be reproducibly fabricated using this process.

Figure 5-2 shows the fabricated interelectrode distances measured (SEM, Leo 982) for these structures as a function of the patterned distance The data used in each of these plots is the average taken from three rows of devices from the same process run; the standard deviation in both plots was less than 20% The interelectrode distance was found to vary less than 20% in measured sections of each device, however local

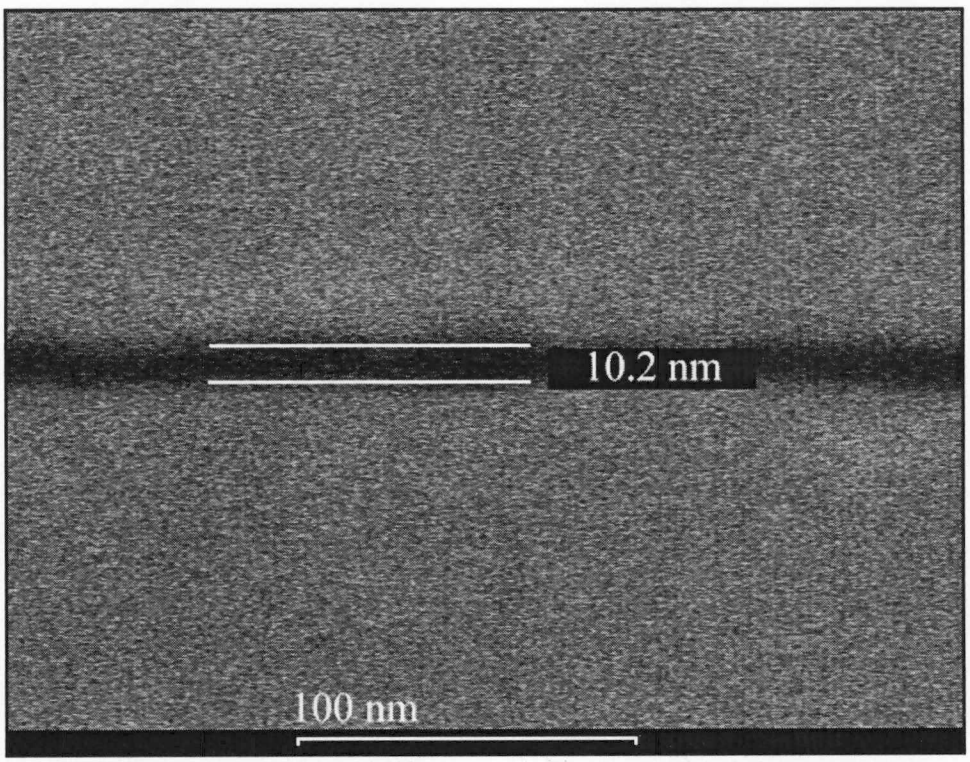

Figure 5-1: Example SEM mircrograph of the smallest interelectrode distance reproducibly fabricated for the bulk effect measurement DiMEND structures. The upper lead shown in this image is Au, the lower lead is Pt.

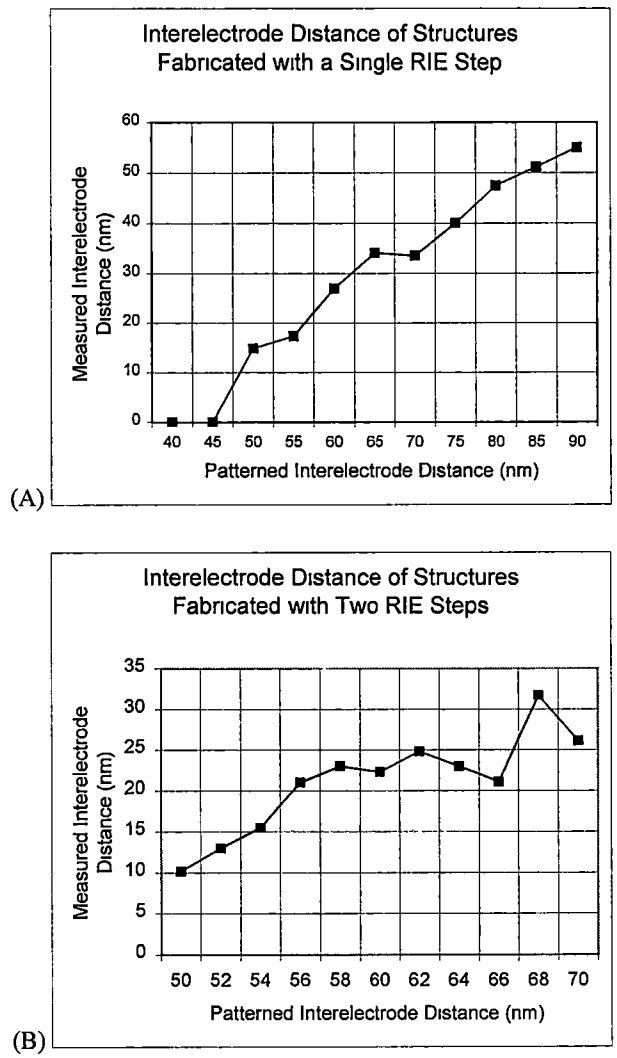

Figure 5-2: Measurements of the interelectrode distance of the bulk measurement DiMEND structures as a function of the patterned interelectrode distance (A) Represents data taken from structures that only experienced one RIE step during processing (B) Displays data taken from structures that underwent RIE prior to both metallization steps While the control of the interelectrode distance is somewhat degraded by this process, the minimum distance was decreased by an average of 5 nm

constrictions and sites with larger separations were periodically observed most likely due to liftoff effects. It is clear from this data that the interelectrode distance of this structure is controllable in roughly 5 nm increments

The plot shown in 5-2(a) represents data taken from structures that only experienced one RIE step during processing (prior to the metallization of the Pt line). The first two data points in 5-2(a) show that the placement of electrodes at distances less than 50 nm resulted in shorted electrode pairs where no gap could be observed over a significant distance. The degraded control of the interelectrode distance indicated by the plot shown in 5-2(b) is most likely attributed to the use of RIE prior to both metallization steps The RIE process introduces some uncertainty into the control of the interelectrode distance. However, this aspect of the process plays a role in allowing the fabrication of electrodes at distances on the order of 10 nm for this structure. This is suggested by the decrease in minimum interelectrode distance achieved between the two process runs shown in 5-2(a) and 5-2(b); both were patterned at a 50 nm separation

An entire wafer of these structures with interelectrode distances ranging from 10 nm to 30 nm was fabricated using RIE prior to both metallization steps. From this wafer, a yield of better than 80% was observed. The most common mode of structure failure was shorted electrodes, occurring most frequently in the first and second columns. Of these columns, only 50% of the devices were found to be useable Shorted electrode pairs were often shown to exhibit high series resistances greater than 10 MΩ indicating that conduction was occurring at a limited number of points along the 300-μm length of the parallel electrodes. During process development it was found that electrode shorting

due to lithography errors resulted in series resistances of less than 10 KΩ. This implies that the main mechanism of electrode shorting on this wafer is not related to the lithography and can most likely be attributed to liftoff effects In particular it was found that the deposited metal had a tendency to bridge the electrode pair at the ends during liftoff This problem was addressed in the production of this wafer by changing the CAD pattern for the electrode pair to include beveled edges (refer to figure 5-3).

The leakage current between the electrodes of useable structures throughout the fabricated size range was measured to be in the femtoampere to picoampere range at bias voltages of - 7 V to .7 V These measurements were performed using an HP 4156 Precision Semiconductor Parameter Analyzer and a Signatone probe station Leakage paths were occasionally created during the removal of the ESD protection resistor trace This was attributed to metal from the trace making contact to the Si substrate on one or both sides of the scribe mark This problem was avoided by taking care not to apply too much pressure during the removal of the trace

One flaw in the original DiMEND process was brought to light while attempting to package the structures using thermosonic Au ball wire-bonding. During the bonding process, the non-Au metal electrode would become damaged at the point where it overlapped the macroscopic Au trace that formed the connection from the fine geometry electrode to the probing pad (refer to figure 5-4). This was believed to be a consequence of the mechanical instability created by depositing a thin metal film via PVD over the step edge created by the predefined macroscopic Au electrode. This hypothesis was supported by the fact that the fine geometry Au electrode was never found to be damaged

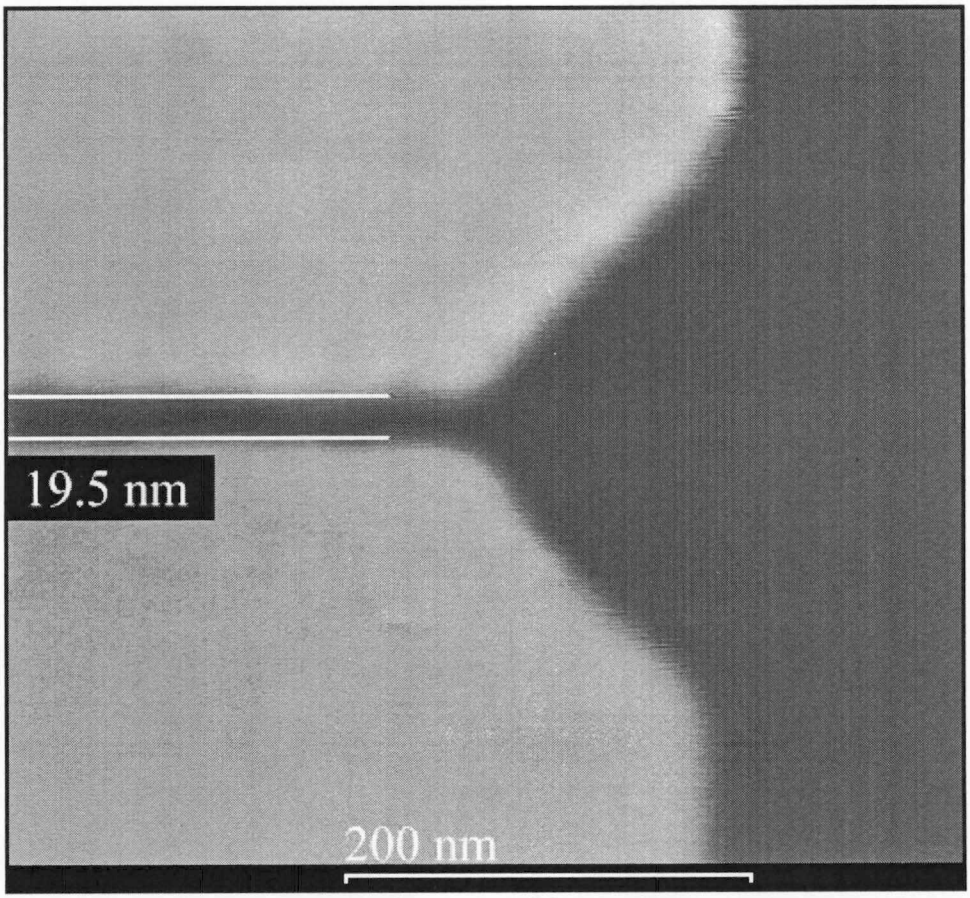

Figure 5-3: SEM micrograph of the end of an example bulk measurement DiMEND structure showing the beveled electrode edges. This change in the CAD pattern helped to prevent the electrode pairs from being shorted out by metal debris during lift off.

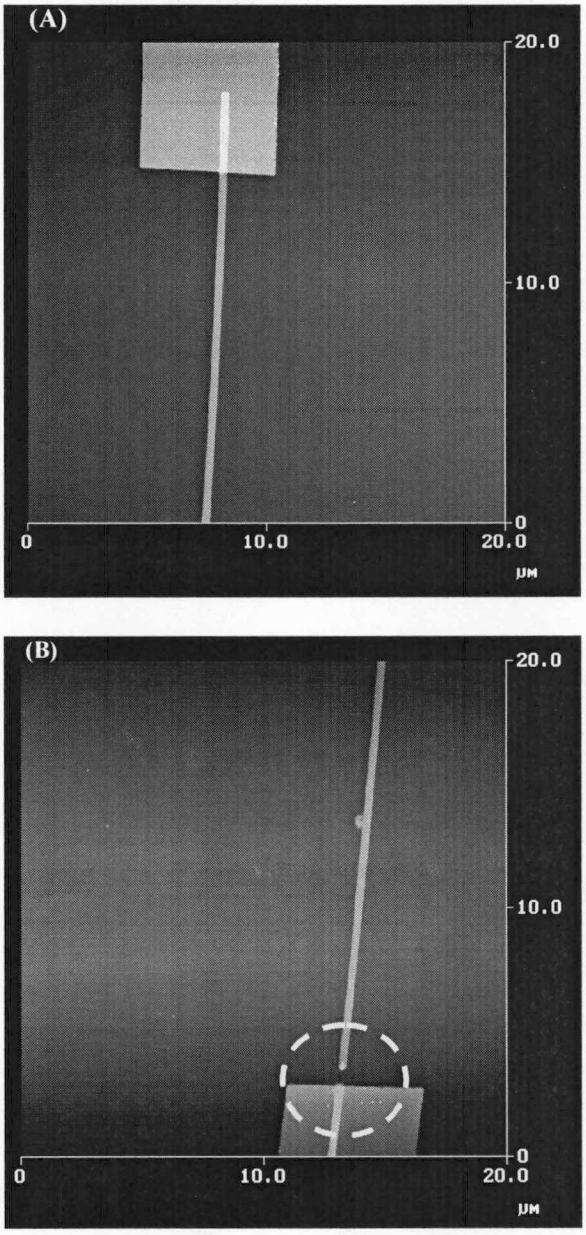

Figure 5-4: AFM scans of the interface between the non-Au electrode and the macroscopic Au lead. In (A) a structure before wirebonding is shown, (B) shows this same structure after wirebonding. The damaged point is circled.

during this procedure The major difference between the fabrication of the Au and non-Au electrodes was that the Au electrodes were patterned and metallized at the same time as the macroscopic Au leads, avoiding the creation of this point of instability.

In order to package these structures, a wirebonding process that did not use any form of excessive mechanical agitation was developed. This involved using a conducting epoxy (Tra-Con Bipax Silver Epoxy) to physically glue wires to the probing pads on each structure (refer to figure 5-5). This process was time consuming and difficult to master but was never found to damage the electrode pair.

5.2 Single PSI Measurement DiMEND

Two different methods were used to fabricate the single PSI measurement electrodes. The first method utilized the DiMEND process as discussed in Chapter 4. The second method incorporated two changes in order to make the process more robust, thereby realizing structures that could be reliably packaged using standard wirebonding techniques. The first change was the creation of a third registered EBL patterning step through the separation of the coarse and fine feature exposures in the first patterning step discussed in 4 3. The process flow was modified such that the fine geometry electrodes were patterned and metallized prior to the patterning and metallization of the bonding pads, macroscopic leads and the ESD protection resistor The second change was to the CAD pattern of the fine geometry electrodes. This change will be discussed in greater depth later in this chapter

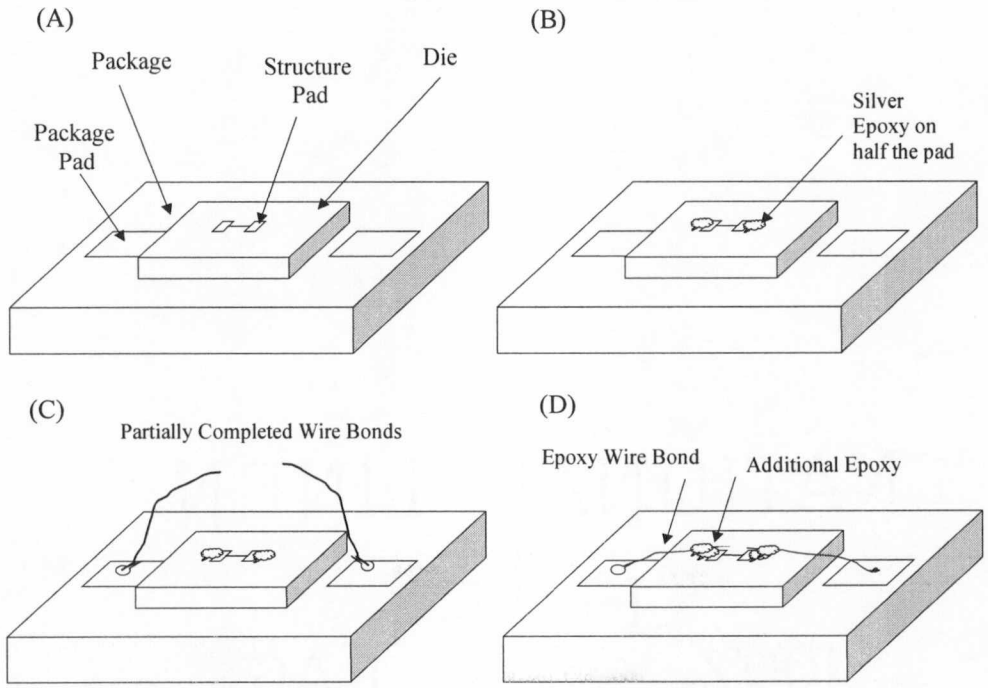

Figure 5-5: Epoxy Packaging Technique. (A) The die is fixed to the package with conducting silver epoxy. (B) The probing pads are partially coated with the epoxy to increase the size of the contact area. (C) Partial wire bonds are made to the package without terminating the bond on the die. (D) Tweezers are then used to place the bond on the epoxy coated pad. Additional epoxy is then used to fix the bond in place.

5.2.1 Results Using the Original DiMEND Process

The single PSI measurement structures fabricated using the original DiMEND process were designed to have a 10 nm interelectrode distance, which was thought to be the ideal interelectrode distance for making direct electrical contact to a limited number of PSI biomolecules Smaller interelectrode distances were fabricated to find the lower limit of this process by varying the interelectrode distance from column to column as described in 5.1. Four different sets of electrodes of this variety were fabricated, each containing one electrode of Au and a second electrode of Pt, Ti, Pd or Al Wafers with two 5x10 arrays of structures were fabricated where the upper and lower arrays were created in different process runs.

The production of this second set of DiMEND structures presented a different host of processing issues compared with the first There was no need to provide manual correction for proximity effect in the placement of the two electrode tips. The interelectrode distance specified in the pattern generation file for the VB6 was less than 15% different from the physically realized structure and often exactly the same for distances of 10 nm or more. Adhesion of the fine geometry electrode metal became an issue and detracted significantly from the initial process yield of less than 30%. It was found that this was largely due to excessive ultrasonic agitation during liftoff. Reducing the time of the ultrasonic agitation to 30 s or less provided adequate removal of the PMMA without introducing significant damage to the electrode pairs. Finally, it was found that the ability to achieve the desired electrode tip geometry was primarily a

function of the metal grain size. This was particularly difficult to control in the case of the Au electrode as this material exhibits an inherently large grain structure when deposited via thermal evaporation Evaporation rates of 10 Å/s in a vacuum of 1×10^{-6} Torr were found to yield acceptable results.

The high level of correlation between the designed and physically realized interelectrode spacing observed in the fabrication of the bulk measurement DiMEND structure was not seen in the fabrication of single PSI measurement DiMEND. As noted previously, the majority of the structures were designed to have an interelectrode spacing of 10 nm, and this was reflected in the yield of the optimized process However, the linear trend across rows where the interelectrode distance was changed incrementally was not observed. The overall structure yield per process run was close to 70%, with adhesion problems remaining as the dominant process variable This resulted in either discontinuous electrodes or interelectrode distances greater than 15 nm, exceeding the range of interest. These difficulties may be attributed to the design of the electrode geometry The electrodes were patterned as simple 75 nm wide rectangular lines that extended over 50 μm Features this fine that extend over several microns are typically difficult to fabricate in high yield as the probability that defects in the features will occur scales with the length of the features

Measurement of the interelectrode distance via SEM was necessary to identify useable structures This detracted from the process throughput and raised issues about sample contamination. O_2 plasma cleaning of the structures was found to sufficiently remove contamination without damaging the electrodes at the cost of added process

complexity Interelectrode distances of 6 nm were reproducibly fabricated and measured using two different SEM systems (Leo 982 and Hitachi S4700) An example of such a structure is shown in figure 5-6. Electrode pairs with smaller interelectrode spacing could not be measured clearly in either SEM However, electrical measurements made on these structures indicate that they are electrically isolated, showing interelectrode currents in the femtoampere to picoampere range at bias voltages of -.7 V to 7 V. This puts the lower bound of this process somewhere below 6 nm, and is yet to be determined.

These structures were even more difficult to package then the bulk measurement DiMEND. In addition to the mechanical instability of the overlap between the non-Au electrode and the macroscopic Au leads, the tips of the electrodes also proved to be mechanically unstable. Thermosonic Au ball bonding and Al wedge bonding to the Au electrode resulted in obliteration of the electrode tip (refer to figure 5-7) This problem relates to the CAD pattern for the fine geometry electrode Structures with wider leads (200 nm and greater) had been packaged without damaging the electrode tip in previous experiments Also, structures with angular bends or kinks in them had been packaged using standard wirebonding techniques (refer to figure 5-8) The CAD pattern for these electrodes had neither of these features The epoxy-based wirebonding technique was successful in packaging these structures Once again, it should be emphasized that this process is both difficult and tedious.

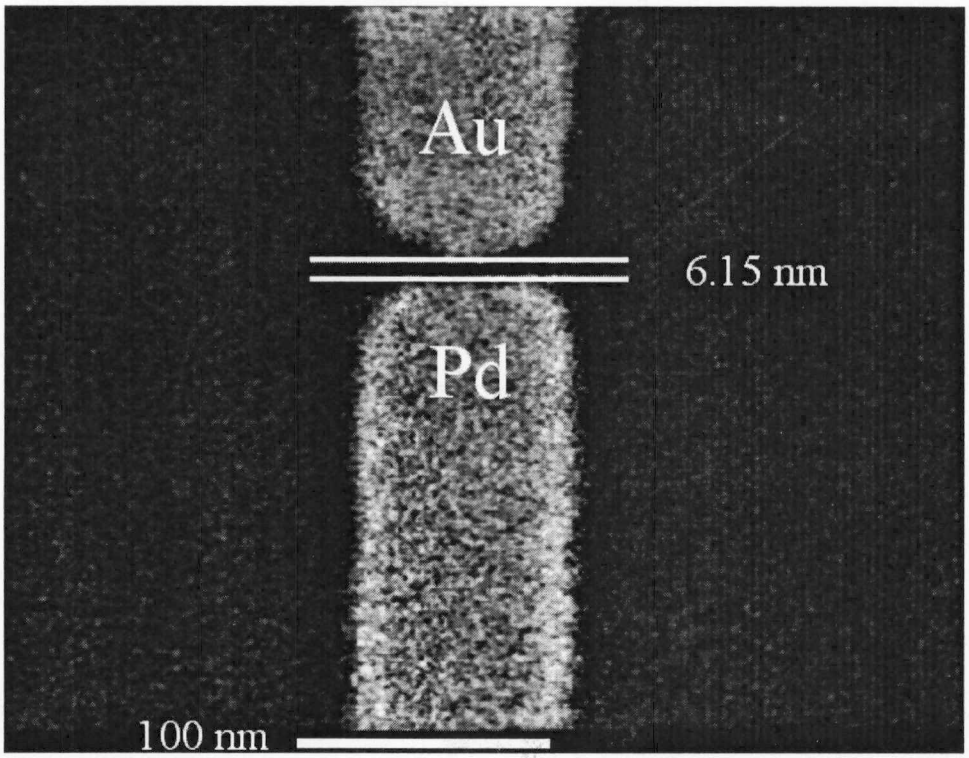

Figure 5-6: Example SEM micrograph of the smallest reproducibly fabricated single PSI measurement DiMEND using the original process.

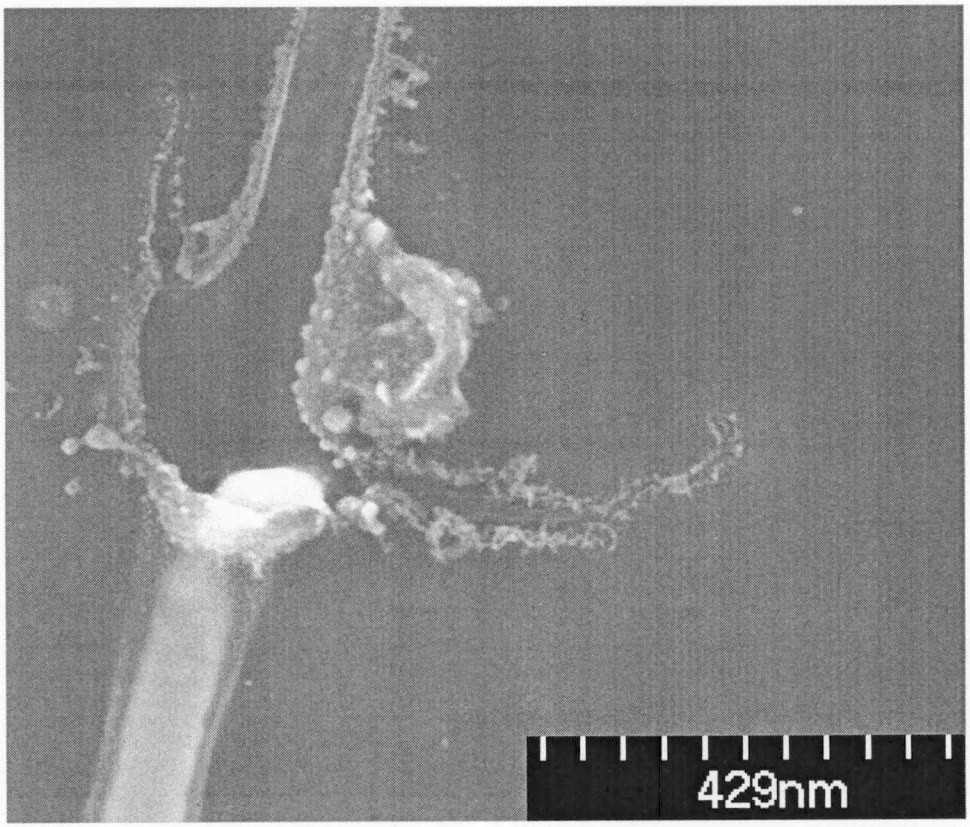

Figure 5-7: SEM micrograph of a single PSI measurement DiMEND after wirebonding. The obliterated lead at the top of the image is the Au electrode tip. Note that the non-Au electrode is not damaged at the tip. This electrode was damaged at the macroscopic Au lead/non-Au fine geometry electrode interface, preventing it from being damaged at the tip.

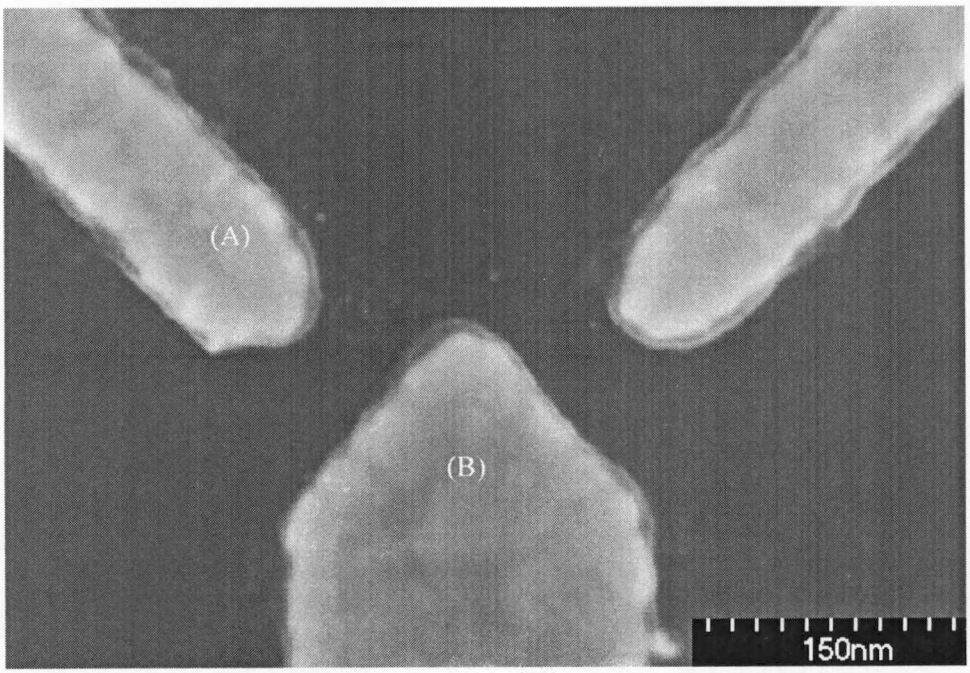

Figure 5-8: SEM micrograph of the three terminal structure after wirebonding. The mechanical instabilities seen in the previous structures have been avoided due to the 45° bend in the leads (A) and the increased width of the electrodes (B). In addition, the fine geometry metal does not overlap the macroscopic leads of this structure; the entire structure was fabricated from Au in a single layer patterning process.

5.2.2 Results Using the Modified DiMEND Process

The DiMEND process was modified to correct for the flaws that complicated the packaging of these structures. These modifications were briefly discussed in 5 2 but will be treated here in greater depth. As described earlier, the DiMEND process flow was changed by the creation of a third registered EBL patterning step through the separation of the coarse and fine feature exposures in the first patterning step discussed in 4.3. In the modified process, the fine geometry electrodes were patterned and metallized prior to the patterning and metallization of the bonding pads, macroscopic leads and the ESD protection resistor. This allowed for a thicker, more mechanically stable film to be deposited onto the fine geometry features of the electrode pair, literally burying the overlapping points A metallization of 50 Å of Cr and 650 Å Au was used, avoiding the problems associated with the step coverage of thin films deposited via PVD

The second modification was to the CAD pattern for the fine geometry electrodes This included widening the main portion of the electrode leads to 250 nm, shortening the length between the electrode tip and the macroscopic leads and incorporating a bend in the electrode for improved mechanical stability.

The results seen in structures fabricated using this process were somewhat different from those fabricated using the original DiMEND process Most notably, adhesion problems were virtually eliminated from the process yield This allowed the observation of a distinct linear trend in interelectrode distance in rows were this distance was incrementally changed by 2 nm. Shown in figure 5-9 are sample images taken from

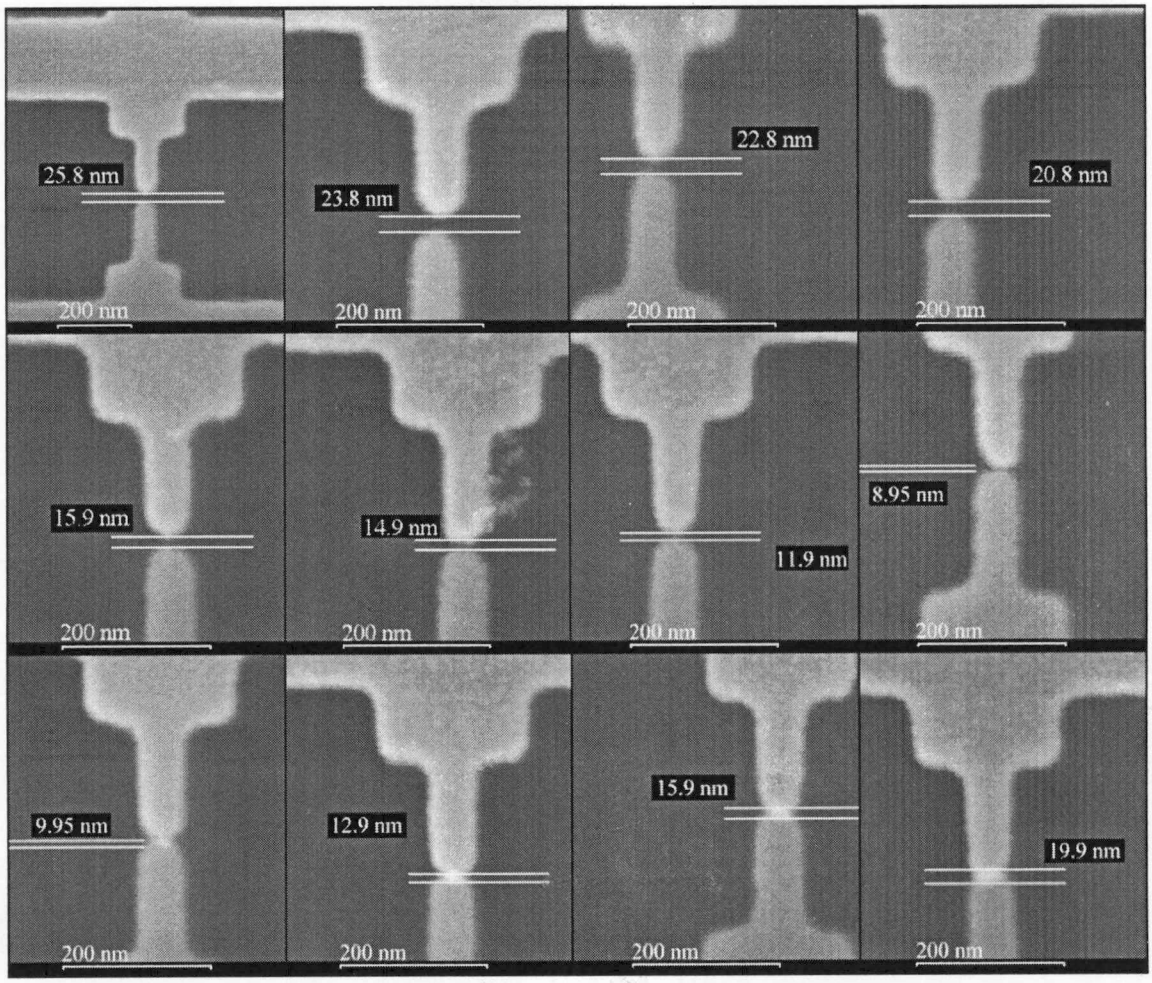

Figure 5-9: Sample SEM micrographs from an array of structures patterned at interelectrode distances from 40 nm to 80 nm. The upper electrode material in each image is Au while the lower electrode is composed of Ti. The specified interelectrode distance decreases from top to bottom and from left to right. Note that the measurements shown in the bottom row indicate the distance of electrode overlap.

two rows where the interelectrode distance was decreased from column to column over the entire 20-element array Shown in figure 5-10 is the data from SEM measurements of the structures across the complete array.

Figure 5-9 clearly shows that the interelectrode distance is controllable to below 9 nm at a patterned interelectrode spacing of 20 nm before shorting them out lithographically The minimum observed interelectrode distance in these arrays was somewhat higher than that seen in the original DiMEND process. This might be merely a metrology problem as the Leo 982 SEM used to carry out this task was in sub-optimal working condition at the time these measurements were made Measurements taken from other structures patterned at a 19 nm to 16 nm interelectrode distance were inconclusive as to whether or not the electrodes were shorted together Electrical characterization of these structures has not yet been performed

Leakage current measurements on these devices were identical to those performed on the structures fabricated using the original DiMEND process. However, unlike the original structures, Al wedge bonding without damaging the electrode structure in any observable way was possible Shown in figure 5-11 is a SEM micrograph of an example structure after Al wedge bonding

5.3 Four Terminal DiMEND

Unlike the previous two DiMEND structures, where the interelectrode distance was varied by adjusting the placement of the two electrodes with respect to one another,

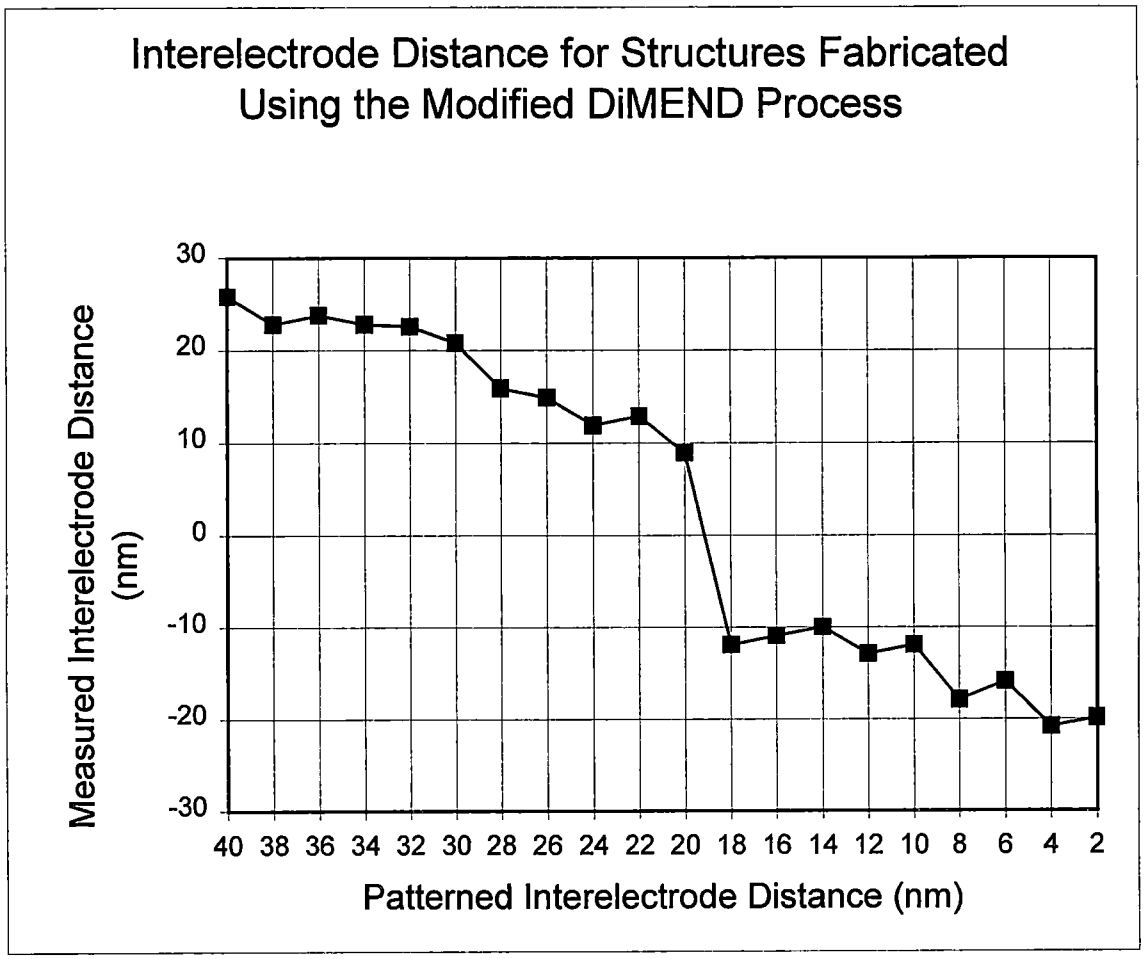

Figure 5-10· Measurement of the observed interelectrode distance as a function of the patterned interelectrode distance for single PSI measurement structures fabricated using the modified DiMEND process. The negative values indicate overlap of the electrode tips

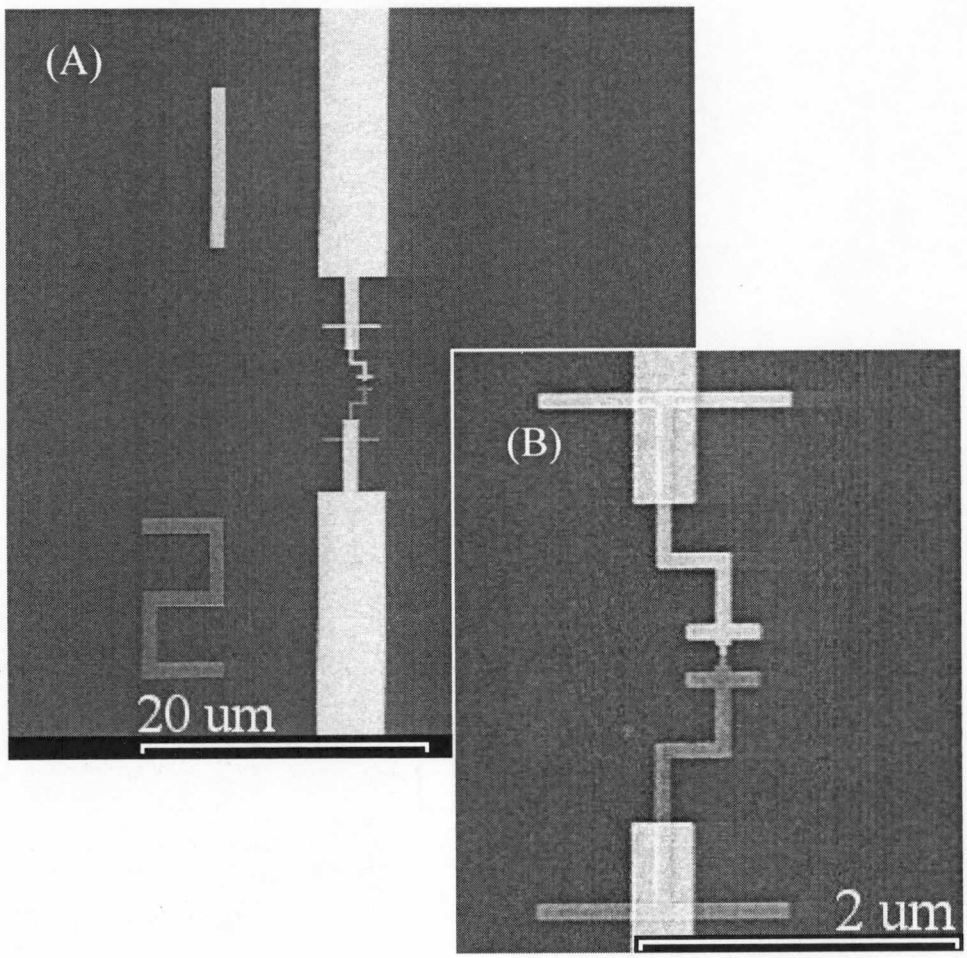

Figure 5-11: SEM micrograph of a completed single PSI measurement structure after Al wedge bonding to an external package.

control of the interelectrode distance here was achieved by incremental change of the exposure dose of the Au electrode. This resulted in Au electrode widths ranging from 90 nm to 110 nm in a nonlinear fashion and interelectrode distances from 18 nm to 8 nm.

The processing issues associated with this structure were slightly different from that of the single PSI measurement DiMEND Out of a 6x10 array of these structures, where the width of the Au electrode was varied from column to column, the structure yield was close to 100% in terms of whether the structure had at least one useable electrode pair of the patterned dimension. However, some structures showed individual electrodes that had adhesion problems resulting in a three or two terminal structure This occurred in less than 30% of the structures

The mechanism used to vary the interelectrode distance was more difficult to control than the method used in the previous two structures The distance between the Ti electrodes perpendicular to the Au electrode was relatively symmetric and within 15% of the patterned distance The Ti electrode in line with the Au was typically closer to the Au than the other two Ti electrodes. Structures with reasonably symmetric interelectrode distances were observed for distances of 10 nm or more (refer to figure 5-12) Interelectrode distances as low as 8 nm could be reproducibly fabricated between the Au and Ti electrodes with a minimum observed distance of 6 nm Attempts to pattern electrodes with interelectrode distances less than 6 nm resulted in shorted electrode pairs

Much like the other two DiMEND structures discussed in this thesis, this structure was unable to survive standard packaging techniques. Unlike the first two structures the epoxy wire-bonding technique could not be used to package this device The epoxy

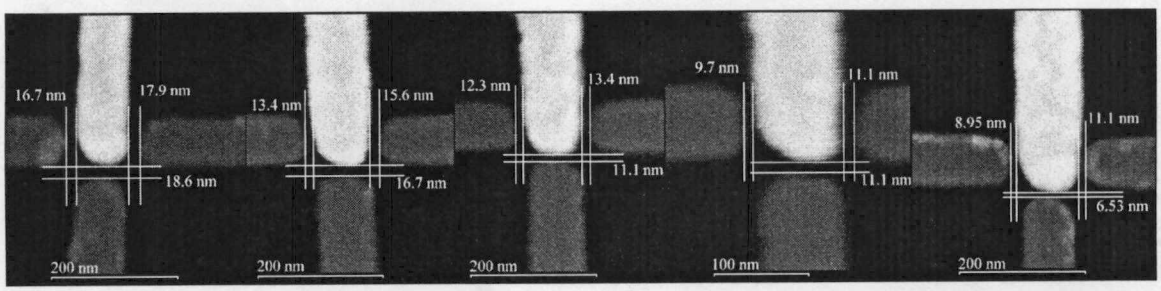

Figure 5-12: Sample SEM micrographs of the four terminal DiMEND structure. These devices were contained in the same wafer row. The dose of the Au line, and hence the line width, increases from left to right. Note: the fourth image from the left was taken at a higher magnification than the other four images.

would consistently short two or more of the terminals together as it is quite difficult to control exactly where it gets deposited. The modified DiMEND process may remedy this situation This has not yet been attempted.

Chapter 6

Conclusion

The production of electrode structures suitable for making electrical measurements on single molecule devices has been a major obstacle in the path towards achieving functional molecular-scale electronic systems. This has largely been a consequence of the lack of standard processing techniques capable of realizing such structures. While several methods for fabricating novel structures to characterize molecular electronic devices have been developed and successfully demonstrated, most do not offer a high degree of latitude in terms of the types of molecular devices they may be used to examine, or the materials from which they can be constructed.

Presented in this thesis is a technique capable of producing planar electrode structures with interelectrode distances below 6 nm This technique can be used to produce electrodes of dissimilar metals that may allow the use of self-assembled monolayer based surface modification chemistry to deposit molecules with asymmetric electrical properties into metal/molecular monolayer/metal heterojunctions These structures have been successfully fabricated from a variety of materials including, Au, Pd, AuPd, Ti, Al, and Pt. However, theoretically any material that is compatible with standard liftoff processing can be used to construct these devices

The application of this technique to the PSI reaction center was examined and should provide a means with which to perform electrical characterization of this

biomolecule. Preliminary data suggests that the PSI molecule can self-assemble on the sides of step edges not unlike those present at the tips of the electrodes The preferential self-assembly of the PSI to substrates of dissimilar metals has also recently been examined. This data indicates that while the thiol-based surface modification chemistry works effectively to assemble oriented PSI on Au and AuPd, it does not function nearly as well on Ti and Pd[86] Work on implementing the DiMEND structures to electrically characterize the PSI has already begun and will constitute the next major phase of this research

The ability to produce multi-terminal structures such as the four-terminal DiMEND presented in this thesis represents a significant advance in the field of molecular scale electronics It provides a means of potentially realizing a multilevel diode-resistor logic gate with an active area much less than 500 nm on a side (refer to figure 6-1)

The DiMEND process utilizes standard processing techniques that are well known to the microelectronics community. The most complicated part of the DiMEND process is the high-resolution EBL patterning step With a well-maintained commercial EBL system such as the Leica VB6, even this portion of the process is relatively easy to implement. This allows the DiMEND process to produce wafer-scale quantities of electrode structures in a single day's time unlike many of the other fabrication techniques presented for similar structures.

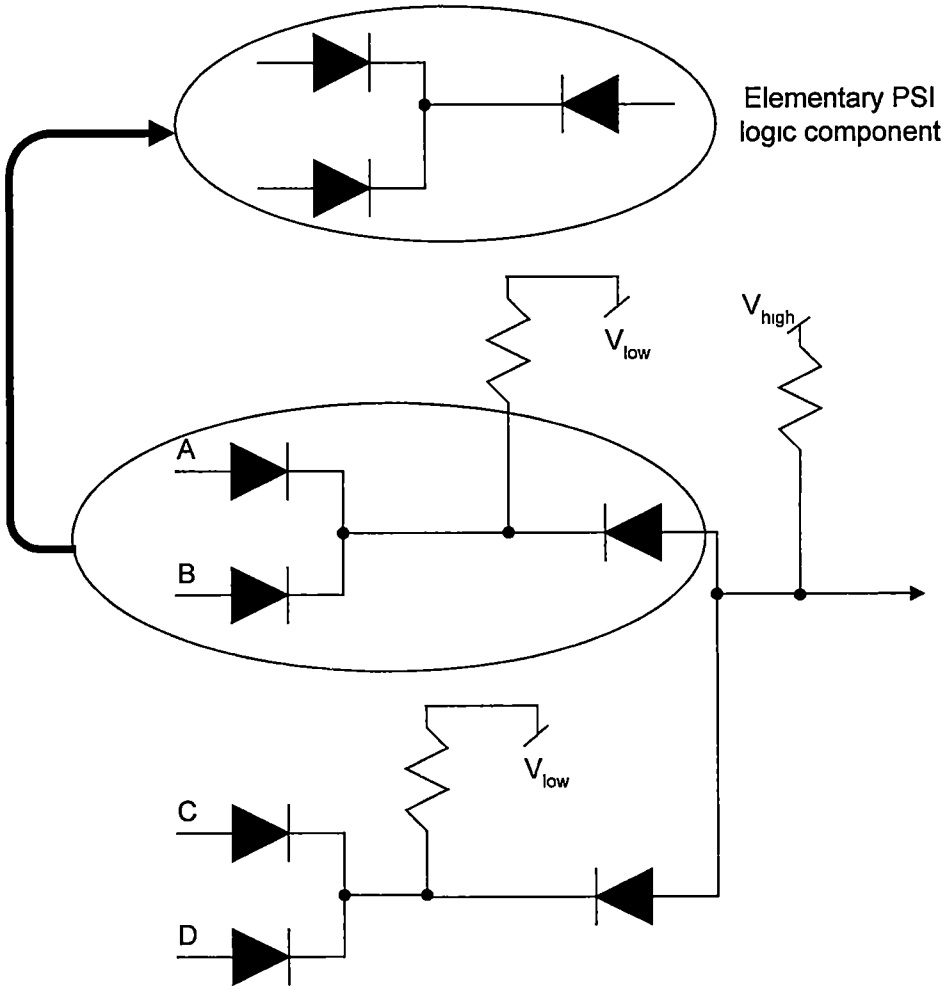

Figure 6-1 By combining two of the four terminal DiMEND structures together a Boolean 2-OR/AND structure may be fabricated with an active device area less than 500 nm on a side

The main drawback of the DiMEND process is that it is dependent on the robust alignment capabilities of the VB6. This work has demonstrated this system's ability to register to preexisting features with less than 5 nm of misalignment, which is a crucial part of the DiMEND process. The availability of this tool to the industrial, government and academic research communities through the National Nanofabrication User's Network makes this process a viable research technique. Other high-resolution EBL systems such as the Leica EBPG 5000+[87] and the JEOL 6000FS and 9300[88] should be capable of achieving similar results as they offer similar operating specifications as the VB6. It may also be possible to produce similar structures with lower cost SEM based EBL systems, investigation by the author into this possibility is already underway.

List of References

List of References

[1] G. Timp Nanotechnology, New York: AIP Press, 7 (1999)

[2] Computation efficiency as defined by binary arithmetic operations per Joule at room temperature

[3] The 1999 National Technology Roadmap for Semiconductors is a publication of the Semiconductor Industry Association and is available through their website· www sematech org

[4] I. Hiroshi, IEEE J. Solid State Circ , **34**, 357 (1999)

[5] R. R. Schaller, IEEE Spectrum, **34**, 53 (June 1997)

[6] J. Heath, P. Kuekes, G Snider, R S Williams, Science, **280**, 1716 (1998)

[7] Feynman's speech can be found at http //nano xerox.com/nanotech/feynman.html

[8] A Aviram, M Ratner, Chem Phys. Lett., **29**, 277 (1974)

[9] S Roth, S, Blumentritt, *et al*, Synthetic Metals, **94**, 105 (1998)

[10] A S. Martin, G. J Ashwell, *et al*, Phys. Rev. Lett., **70**, 218 (1993)

[11] C. M Fischer, M Burghard, *et al*, Appl. Phys Lett , **66**, 3331 (1995)

[12] D. Vuillaume, R Metzger, *et al*, Langmuir, **15**, 4011 (1999)

[13] A Aviram, C Joachim, *et al*, Chem. Phys. Lett., **146**, 490 (1999)

[14] A Stabel, J. P. Rabe, *et al*, Angew Chem. Int Ed. Engl., **34**, 1609 (1995)

[15] I Lee, J. Lee, E. Greenbaum, *et al*, Proc Natl Acad Sci , USA, **92**, 1965 (1995)

[16] L A. Bumm, J. J Arnold, J M. Tour, P. S. Weiss, *et al*, Science, **271**, 1705 (1996)

[17] M A. Reed, Proc IEEE, **87**, 652 (1999)

[18] J Chen, M A. Reed, A. M. Rawlett, J. M Tour, Science, **286**, 1550 (1999)

[19] For example see M.S. Dresselhaus, G. Dresselhaus, P.C. Ecklund, Science of Fullerenes and Carbon Nanotubes, New York. Academic Press, (1995)

[20] S. Chu, Reviews of Modern Physics, **70**, 685 (1998)

[21] G L Gaines, Insoluble Monolayers at Liquid-Gas Interfaces, New York: John Wiley & Sons (1966)

[22] This includes colloidal suspensions of single molecules or nanoparticles.

[23] C J Muller, R. de Bruyn Ouboter, J. Appl Phys., **77**, 5231 (1995)

[24] M. A. Reed, J M. Tour, *et al*, Science, **278**, 252 (1997)

[25] For a review refer to J L Wilbur, G. M Whitesides, Nanotechnology, New York: AIP Press, Chapter 8 (1999)

[26] A. P. Alivisatos, P. L McEuen, *et al*, Appl Phys Lett , **75**, 301 (1999)

[27] K. S Ralls, R. C Tiberio, *et al*, Appl. Phys Lett , **55**, 2459 (1989)

[28] C Zhou, M A Reed, J M Tour, *et al*, Appl Phys. Lett , **71**, 611 (1997)

[29] M. A Reed, J M Tour, *et al*, Annals New York Academy of Sciences, **852**, 133 (1998)

[30] A Bezryadin, C. Dekker, Appl. Phys Lett , **71**, 1273 (1997)

[31] PMMA is a standard high resolution EBL resist

[32] This technique was recently used by Dekker, *et al*, to make electrical measurements on DNA However, the electrical properties of DNA are not dependent upon orientation, though it is a highly polar molecule Refer to D. Porath, A. Bezryadin, S. de Vries, C. Dekker NATURE, **403**, 635 (2000).

[33] G J Dolan, Appl. Phys Lett , **31,** 337 (1977)

[34] for example see D.L Klein, P.L. McEuen, *et al*, Appl. Phys Lett., **68**, 2574 (1996)

[35] T. Weimann, H. Wolf, *et al*, Appl Phys. Lett , **71**, 713 (1997)

[36] A. F Morpurgo, C. M Marcus, D B Robinson, Appl Phys Lett **74**, 2084 (1999)

[37] E. DiFabrizio, L Grella, M Gentili, M Baciocchi, L. Mastrogiacomo, P. Morales, Jpn J Appl. Phys, **36**, L70 (1997)

[38] M.A. Guillorn, D.W Carr, R C. Tiberio, E Greenbaum and M L. Simpson, J. Vac. Sci Tech. B, **18**, 1177 (2000)

[39] M J Rooks and M.A McCord, Handbook of Microlithography, Micromachining and Microfabrication Volume 1 Microlithography, Bellingham. SPIE press, 149 (1997)

[40] G Owen and J. Sheats, Microlithography Science and Technology, New York: Marcel Dekker, Inc , 371 (1998)

[41] M J Rooks and M A. McCord, Handbook of Microlithography, Micromachining and Microfabrication Volume 1: Microlithography, Bellingham SPIE press, 149 (1997)

[42] M.J Rooks, M.A McCord, Handbook of Microlithography, Micromachining and Microfabrication Volume 1· Microlithography, Bellingham SPIE press, 150 (1997)

[43] M J Rooks, M A McCord, Handbook of Microlithography, Micromachining and Microfabrication Volume 1: Microlithography, Bellingham· SPIE press, 147 (1997)

[44] M J Rooks, M.A McCord, Handbook of Microlithography, Micromachining and Microfabrication Volume 1· Microlithography, Bellingham SPIE press, 152 (1997)

[45] M J. Rooks, M.A McCord, Handbook of Microlithography, Micromachining and Microfabrication Volume 1· Microlithography, Bellingham. SPIE press, 152 (1997)

[46] M.J Rooks, M.A. McCord, Handbook of Microlithography, Micromachining and Microfabrication Volume 1: Microlithography, Bellingham: SPIE press, 153 (1997)

[47] G. Owen and J. Sheats, Microlithography Science and Technology, New York. Marcel Dekker, Inc , 372 (1998)

[48] M.J Rooks, M.A. McCord, Handbook of Microlithography, Micromachining and Microfabrication Volume 1 Microlithography, Bellingham. SPIE press, 154 (1997)

[49] M.J. Rooks, M.A. McCord, Handbook of Microlithography, Micromachining and Microfabrication Volume 1 Microlithography, Bellingham· SPIE press, 154 (1997)

[50] M.J Rooks, M.A. McCord, Handbook of Microlithography, Micromachining and Microfabrication Volume 1 Microlithography, Bellingham· SPIE press, 155 (1997)

[51] M J Rooks, M.A McCord, Handbook of Microlithography, Micromachining and Microfabrication Volume 1. Microlithography, Bellingham SPIE press, 155-7 (1997)

[52] M.J. Rooks, M A McCord, Handbook of Microlithography, Micromachining and Microfabrication Volume 1: Microlithography, Bellingham· SPIE press, 155 (1997)

[53] M.J. Rooks, M.A McCord, Handbook of Microlithography, Micromachining and Microfabrication Volume 1. Microlithography, Bellingham SPIE press, 158 (1997)

[54] S A Campbell, The Science and Engineering of Microelectronic Fabrication, Oxford Oxford University Press, 211 (1996)

[55] M.J. Rooks, M.A. McCord, Handbook of Microlithography, Micromachining and Microfabrication Volume 1: Microlithography, Bellingham SPIE press, 159 (1997)

[56] M J. Rooks, M.A McCord, Handbook of Microlithography, Micromachining and Microfabrication Volume 1 Microlithography, Bellingham SPIE press, 162 (1997)

[57] S.A. Campbell, The Science and Engineering of Microelectronic Fabrication, Oxford· Oxford University Press, 211 (1996)

[58] S.A. Campbell, The Science and Engineering of Microelectronic Fabrication, Oxford: Oxford University Press, 208 (1996)

[59] M.J. Rooks, M.A McCord, Handbook of Microlithography, Micromachining and Microfabrication Volume 1. Microlithography, Bellingham SPIE press, 176 (1997)

[60] www.cnf cornell.edu/equipment/vb6.html

[61] S.A. Campbell, The Science and Engineering of Microelectronic Fabrication, Oxford Oxford University Press, 213-14 (1996)

[62] M.J Rooks, M.A. McCord, Handbook of Microlithography, Micromachining and Microfabrication Volume 1. Microlithography, Bellingham SPIE press, 201-3 (1997)

[63] M J Rooks, M.A McCord, Handbook of Microlithography, Micromachining and Microfabrication Volume 1 Microlithography, Bellingham. SPIE press, 205 (1997)

[64] S.A. Campbell, The Science and Engineering of Microelectronic Fabrication, Oxford: Oxford University Press, 274 (1996)

[65] www.microfabrication dimes tudelft.nl/publications/nanometer/nanometer html

[66] S A. Campbell, The Science and Engineering of Microelectronic Fabrication, Oxford: Oxford University Press, 275 (1996)

[67] I Lee, J. Lee, E Greenbaum, *et al*, Proc Natl Acad Sci USA, **92**, 1965 (1995)

[68] R C Ford, A. Holzenburg, EMBO, **7**, 2287 (1988)

[69] E. Greenbaum, Science, **230**, 1373 (1985)

[70] E Greenbaum, J. Phys Chem , **94**, 6151 (1990)

[71] J.W. Lee, I. Lee, P.D. Laible, T.G Owens, E Greenbaum, Biophys. J , **69**, 652 (1995)

[72] I. Lee, J. Lee, E. Greenbaum, *et al*, Proc Natl Acad Sci USA, **92**, 1965 (1995)

[73] J Barber, B Anderson, Nature **370**, 31 (1994)

[74] I Lee, J Lee, and E Greenbaum, Phys. Rev Lett , **79**, 3294 (1997)

[75] L E. Gross, Photosynth Res **37**, 103, (1993)

[76] I Lee, J Lee, and E. Greenbaum, Phys. Rev Lett., **79**, 3294 (1997)

[77] J.W Lee, I. Lee, E. Greenbaum, Biosens, Bioelectron **11**, 375 (1996)

[78] I Lee, J Lee, and E. Greenbaum, Phys Rev. Lett , **79**, 3294 (1997)

[79] For a review refer to J L Wilbur, G. M. Whitesides, Nanotechnology, New York· AIP Press, Chapter 8 (1999)

[80] C D Bain, G M. Whitesides, Angew. Chem. Int. Ed Engl. **28**, 506 (1989)

[81] J E Pemberton, M.A Bryant, S L. Joa, S D Garvey, Proc. SPIE. Int. Soc. Opt. Eng (1992)

[82] P Fenter, *et al* Langmuir, **7**, 2013 (1991)

[83] P.E Laibinis, *et al* Langmuir, **7**, 3167 (1991)

[84] W C Bigelow, D L Picket, W A Zisman, J Colloid Interface Sci , **1**, 513 (1946)

[85] T.R. Lee, Pure Appl Chem., **63**, 821 (1991)

[86] I. Lee, M.A. Guillorn, J. Lee, E Greenbaum, unpublished work

[87] M Wijnands, Leica Lithography Systems, private communication

[88] Y. Nakagawa, JEOL Ltd , private communication

Vita

Michael Guillorn was born in Bridgeport, Connecticut on March 22, 1976. He attended public schools in Trumbull, Connecticut graduating from Trumbull High School in 1994 After Attending the University of Massachusetts at Lowell for the Spring and summer semesters of 1994 as a Music Performance major, Michael decided to transfer to Trinity College in Hartford Connecticut after taking the fall semester of 1994 off. At Trinity Michael pursued a Bachelor of Science degree in Electrical Engineering He worked on a number of projects during his tenure at Trinity ranging from mobile robotics to interlayer dielectric materials for microelectronic applications He also participated in several musical ensembles at Trinity and designed the soundscape for a performance art piece during which he performed or conducted music continuously for 9 5 hours. In 1998 he graduated from Trinity with honors, was inducted into Phi Beta Kappa and elected the President's Fellow for engineering by the engineering faculty

Michael entered into the Master of Science program at the University of Tennessee, Knoxville in August 1998 He was awarded a graduate research assistantship from the UT/ORNL Joint Program in Mixed Signal-VLSI and Monolithic Sensors and participated actively in several ORNL research projects in the field of molecular-scale electronics In June 2000 Michael accepted a staff position at ORNL in the Monolithic Systems Development Group of the Instrumentation and Controls Division He is currently pursuing a Ph.D in Electrical Engineering